JOURNAL OF GEOPHYSICAL RESEARCH, VOL. 114, B05302, doi:10.1029/2008JB005881, 2009



# Insight into the origin of the Tengchong intraplate volcano and seismotectonics in southwest China from local and teleseismic data

Jianshe Lei,[1] Dapeng Zhao,[2] and Youjin Su[3]

Received 18 June 2008; revised 22 February 2009; accepted 10 March 2009; published 13 May 2009.

[1] A high-resolution tomographic image of the crust and upper mantle under Yunnan Province in southwest China was determined by using a large number of teleseismic data measured precisely from digital seismograms as well as local- earthquake arrival times recorded by the dense Yunnan seismic network. The grid spacing of the tomographic model is ~70 km × 78 km in the horizontal directions and 4–70 km in depth. Our resulting model shows a clear low-velocity (low-V, <−0.3% with respect to the average one-dimensional velocity model) column extending from the surface down to about 400-km depth under the active Tengchong volcano and some high-velocity (high-V) anomalies existing in the mantle transition zone. Furthermore, the low-V anomaly extends horizontally toward the northeast at ~250- to 400-km depth. Combining our tomographic results with geochemical and geological investigations, we infer that the Tengchong volcano is a rift-related volcano caused by the subduction and dehydration of the Indian plate as well as corner flow in the mantle wedge, though the subducted slab is a continental plate. Our results show that the upwelling flow under Tengchong originates at ~400-km depth. A prominent low-V anomaly along the Red River fault zone extends down to the upper mantle (~100-km depth), reflecting that the Red River fault zone may have cut through the crust to the upper mantle. The two Dayao earthquakes (*M* 6.1 and *M* 6.2) in 2003 occurred on the margin of high-V anomalies and are underlain by a prominent low-V anomaly in the lower crust and upper mantle, suggesting that the Dayao earthquakes may be associated with fluids released from the dehydration of the subducted Indian slab. These results are significantly improved compared with previous studies and provide new seismic constraints on the dynamic processes of the India-Asia collision.

**Citation:** Lei, J., D. Zhao, and Y. Su (2009), Insight into the origin of the Tengchong intraplate volcano and seismotectonics in southwest China from local and teleseismic data, *J. Geophys. Res.*, *114*, B05302, doi:10.1029/2008JB005881.

## 1. Introduction

[2] During the Cenozoic the India-Asia collision not only formed compressional structures in southern Tibet [e.g., *Tapponnier et al.*, 1981, 1990; *England and Houseman*, 1986; *Yin and Harrison*, 2000], but also caused extensional structures in southeastern Asia [e.g., *Harrison et al.*, 1992, 1996; *Wang and Burchfiel*, 1997; *Wang et al.*, 1998] (Figure 1). The active Tengchong intraplate volcano in southwest China is located on the southeastern margin of this collision zone (Figure 1), and its last eruption occurred in 1609. At present, numerous hot springs exist in the Tengchong volcanic field that consists of a gneissic basement with minor amphibolites and is characterized by rift-related volcanic activity over the last ~5 Ma [*Zhu et al.*, 1983; *Yin*, 2000; *Wang et al.*, 2001].

[3] Many studies have been made for the Tengchong volcanic region, and some important results have been obtained. The Tengchong volcanic area exhibits a higher geothermal gradient [*C. Zhao et al.*, 2006], lower seismic velocity in the crust and uppermost mantle [*Wang and Huangfu*, 2004; *Huang and Zhao*, 2006; *Hu et al.*, 2008], and higher ratio of $He^3/He^4$ [*Shangguan et al.*, 2000], suggesting the existence of magma chambers and hot material under the region. However, the origin of the Tengchong volcano is still debated. Some researchers suggested that it is related to the subduction of the Burma microplate down to 400-km depth [*Huang and Zhao*, 2006], while others ascribed its origin to the subduction of the Indian plate down to ~150-km [*Hu et al.*, 2008; *Li et al.*, 2008a] or ~200-km depth [*Wang and Huangfu*, 2004]. Global tomographic models provide no useful information on the volcano because of their lower spatial resolution of 300–500 km [e.g., *Zhao*, 2001, 2004; *Lei and Zhao*,

[1] Seismological Laboratory, Institute of Crustal Dynamics, China Earthquake Administration, Beijing, China.
[2] Department of Geophysics, Tohoku University, Sendai, Japan.
[3] Earthquake Administration of Yunnan Province, Kunming, China.


0148-0227/09/2008JB005881$09.00

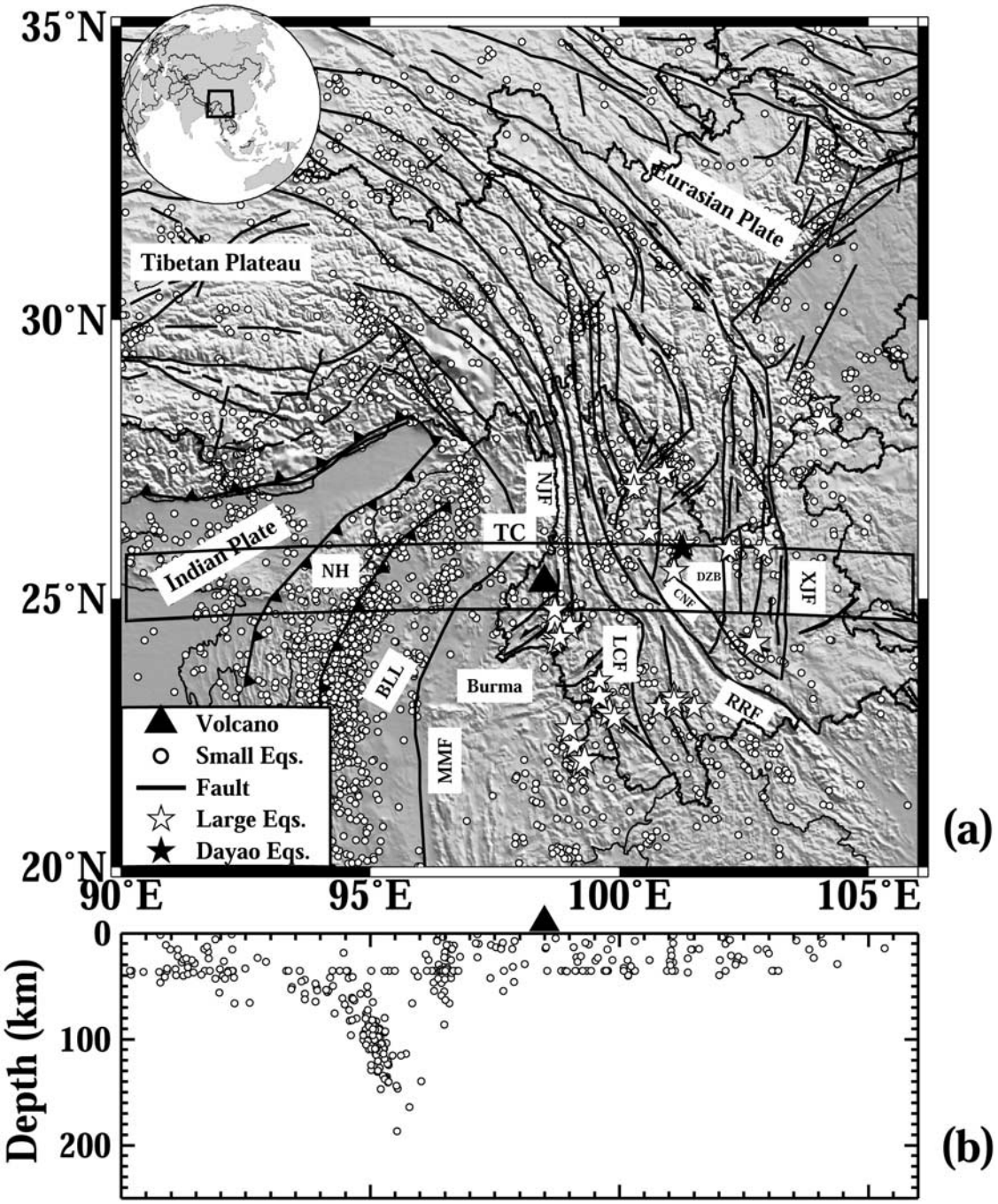


**Figure 1.** (a) Sketch map of tectonic setting around the Tengchong volcano (TC, solid triangle). White dots denote the earthquakes with magnitude greater than 3 during 1964–2004 relocated by *Engdahl et al.* [1998]. White stars denote the strong earthquakes with magnitude larger than 6.0 during 1970–2005, including four earthquakes at the boundary between Yunnan and Burma [*China Earthquake Administration*, 2005], while black star represents the 2003 Dayao earthquakes [*Hua et al.*, 2006]. Major active faults are shown as black lines. NH, Naga Hills; BLL, Burma Lower Lands; MMF, Mandalay-Myityina fault; RRF, Red River fault; NJF, Nujiang fault; XJF, Xiaojiang fault; LCF, Lancang River fault; CNF, Chuxiong-Nanhua fault; DZB, Dian-Zhong block. Insets denote the location of the study area and legend, respectively. (b) Distribution of earthquakes that occurred within the rectangle as shown in Figure 1a.

2006a]. Local tomographic models for this region are valid down to only 80-km depth [e.g., *Huang et al.*, 2002].

[4] With the recent upgrading of 35 seismic stations from analog to digital recording in Yunnan Province, China, since 1998, abundant high-quality local and teleseismic data have been accumulated. In this study, we combined local-earthquake arrival times with teleseismic data recorded by the dense Yunnan seismic network to determine a

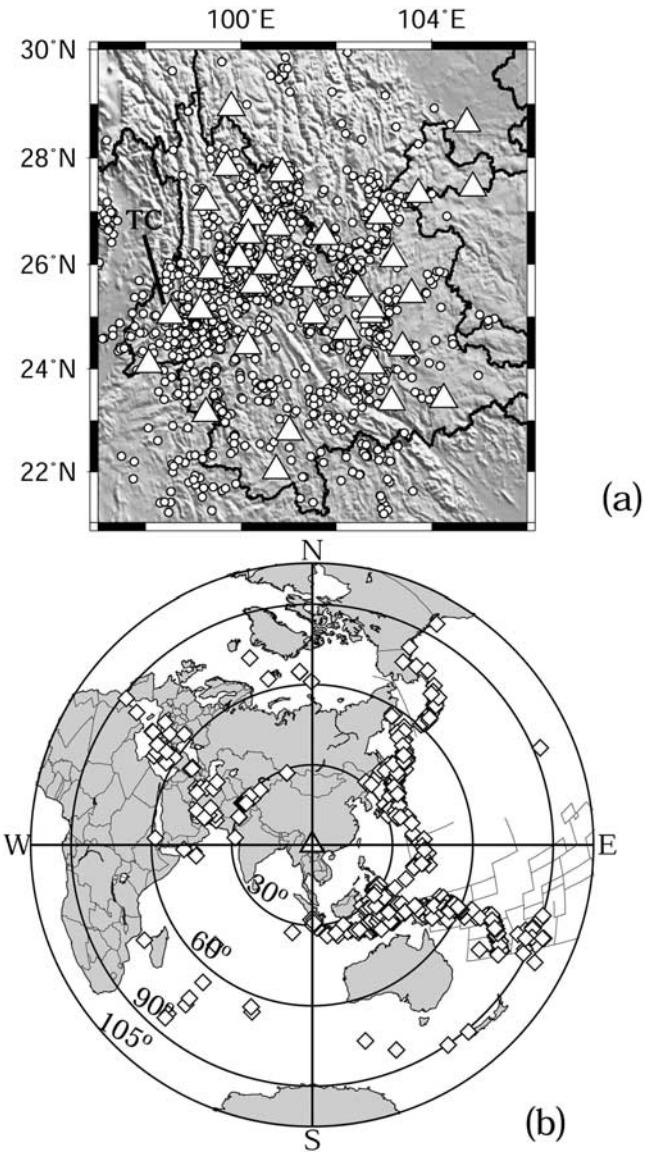


**Figure 2.** (a) Distribution of 35 seismic stations (triangles) and 2761 local earthquakes (white dots) and (b) 602 teleseismic events (diamonds) used in this study. These teleseismic events occurred during 2002–2006. The events before December 2004 were relocated by *Engdahl et al.* [1998], and those after December 2004 were directly downloaded from the Web (http://neic.usgs.gov/neis/epic/epic_global.html). In Figure 2b the numbers represent the epicentral distances (in degrees) from the center (triangle) of the study area. TC, a seismic station in Tengchong.

detailed three-dimensional (3-D) seismic structure of the crust and upper mantle under Yunnan Province. Our results shed new light on the origin of the active Tengchong intraplate volcano.

[5] In the study region there are many active fault zones (Figure 1). The depth extent of these faults including the Red River fault still remains debated. Some researchers infer the Red River fault to be a crustal-scale fault [e.g., *Wang and Burchfiel*, 1997], while others suggested it to be a lithospheric-scale fault [e.g., *Leloup et al.*, 1995]. Over 35 strong earthquakes ($M > 6.0$) occurred in the region since 1970 (Figure 1). Some researchers had discussed the mechanism of these strong earthquakes on the basis of the obtained 3-D velocity structure [e.g., *Huang et al.*, 2002; *Wang et al.*, 2003]. Recently two earthquakes ($M$ 6.1 and $M$ 6.2) occurred in Dayao in the present study area on 21 July and 16 October 2003 successively, which caused 19 deaths and over 600 injuries and resulted in extensive property losses [*Su*, 2004; *He et al.*, 2005]. Therefore in the present study we also discuss the velocity anomalies related to the Red River fault zone and the 2003 Dayao earthquakes.

## 2. Data and Method

[6] Thirty-five seismic stations of the Yunnan seismic network (Figure 2a) are used in this study. Among them, twenty-three stations have been operating since June 1999, but the entire seismic network began to operate in January 2004. Figure 2b shows the epicentral distribution of 602 teleseismic earthquakes used in this study. The magnitude of these events is 5.3 or greater. Each event has at least 8 recordings. These events occurred from January 2002 to December 2006. Among them the events that occurred before December 2004 were relocated by E. R. Engdahl (see the work of *Engdahl et al.* [1998] for the relocation procedure). The teleseismic events selected are located 28 to 96 degrees from the center of the study area and have a good azimuthal coverage, though most of them are distributed around the Western Pacific subduction zones. We measured 11,608 first $P$ wave arrival times from the digital seismograms of the 602 teleseismic events. The data-picking accuracy is estimated to be 0.10–0.15 s. It can be seen from Figure 3 that the teleseismic rays used are nearly vertical, and so it is hard to resolve the crustal structure if only the teleseismic data are used. In order to improve the ray coverage in the crust, we have added local-earthquake arrival times since the local rays are roughly horizontal (Figures 3b and 3c). We collected 17,190 $P$ wave arrival times from 2761 local earthquakes ($M > 2.5$) (Figure 2a). Each local event has at least six recordings, and the picking accuracy of arrival times is estimated to be 0.10 s.

[7] We used the 3-D ray tracer of *Zhao* [2001] in this study. This method cannot only compute the travel times and raypaths accurately and efficiently, but also deal with a model containing complex velocity discontinuities. For details of the technique, see the work of *Zhao et al.* [1992] and *Zhao and Lei* [2004]. Our starting 1-D model (Figure 4) was inferred from previous studies [e.g., *Kan and Lin*, 1986; *Fan and Cheng*, 1992; *Xu et al.*, 2007] for the crust, and the iasp91 velocity model [*Kennett and Engdahl*, 1991] was adopted for the mantle. Depth variations of the Moho discontinuity under the study area (Figure 5) [*Kan and Lin*, 1986; *Xu et al.*, 2007] were taken into account. Travel times were further corrected for the Earth's ellipticity [*Dziewonski and Gilbert*, 1976] and station elevations. Figure 6 shows the distribution of hit counts in map view. Hit counts in the crust amount to over 6000 (Figures 6a–6d), which is higher than in the mantle (Figures 6e–6l). At 70- to 350-km depths the distribution of hit counts is almost uniform in the entire Yunnan Province (Figures 6e–6i), while below 420-km depth the hit counts are biased toward the east (Figures 6j–6l). This pattern is consistent with that of the distribution of raypaths (Figures 3b and 3c), owing to

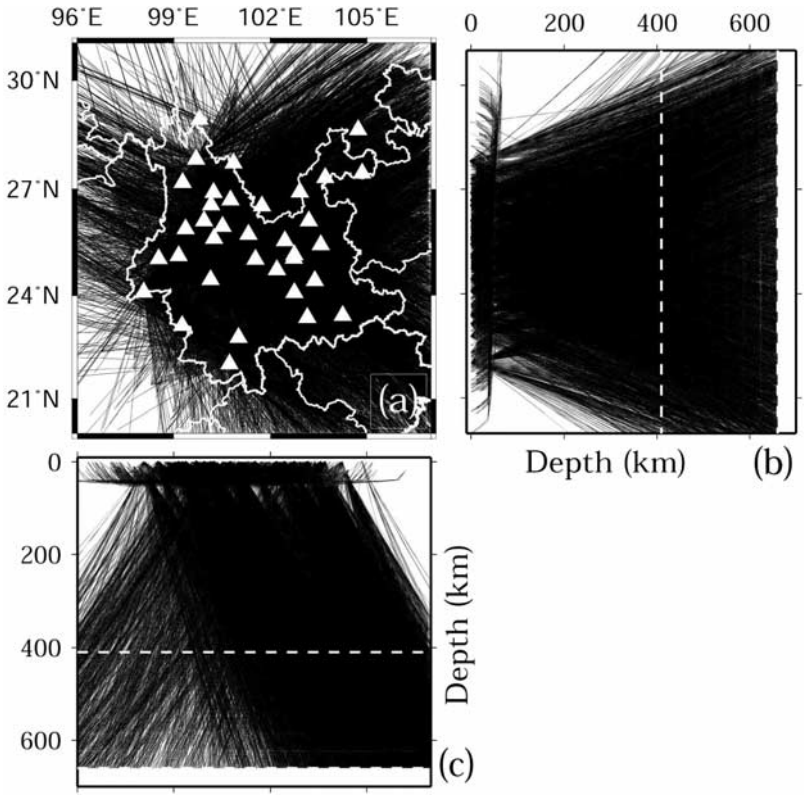


**Figure 3.** Distribution of *P* wave raypaths used in this study in (a) map view, (b) north-south side view, and (c) east-west side view. White triangles denote the seismic stations used in this study. White curves denote the national borders and the boundaries between different provinces of China. White dashed lines in Figures 3b and 3c denote the 410-km discontinuity.

the occurrence of comparatively many teleseismic events in the Western Pacific subduction zones (Figure 2b).

[8] We applied the tomographic method of *Zhao et al.* [1994] to 11,608 relative traveltime residuals from teleseismic events and 17,190 absolute traveltime residuals from local earthquakes to determine the 3-D crust and upper mantle structure under Yunnan. The use of the relative traveltime residuals from teleseismic events in the tomographic inversion can minimize the effects of the uncertainties in hypocentral parameters, as well as the velocity heterogeneity outside the study area. For details of the calculation of the relative traveltime residuals, see the work of *Zhao et al.* [1994] and *Lei and Zhao* [2005, 2007b]. Figure 7 shows the distribution of relative traveltime residuals versus the epicentral distance. It can be seen that over 95% of the residuals are concentrated in the range of −1.0 to 1.0 s. Therefore, in this study we used only relative residuals located in this range, and the final number of the teleseismic data used in the inversion is 11,608.

[9] Figure 8 shows the distribution of the average relative traveltime residuals at every station for all the teleseismic events, which range from −0.5 to 0.5 s. Delayed arrivals are visible at stations in eastern Yunnan, suggesting the existence of low-velocity (low-V) anomalies there in the upper mantle. Early arrivals appear at most stations in western Yunnan, indicating that high-velocity (high-V) anomalies exist in the upper mantle under the region. But some stations in the Tengchong volcanic area in western Yunnan exhibit delayed arrivals, suggesting that low-V anomalies also exist there. To understand how such a pattern of relative traveltime residuals in the region is formed, we show the distribution of the relative residuals per source quadrant in Figure 9. There exist some significant differences in the pattern of residuals between the NW and SW quadrants (Figures 9a and 9c) and between the NE and SE quadrants (Figures 9b and 9d), which reflect the different angles of rays emerging from the events in different source-quadrants. However, some features are similar between the NW and NE quadrants (Figures 9a and 9b) and between the SW and SE quadrants (Figures 9c and 9d). In the NW and NE quadrants some stations in the Tengchong volcanic area in western Yunnan exhibit delayed arrivals (Figures 9a and 9b), while in the SW and SE quadrants most of the stations in eastern Yunnan show delayed arrivals (Figures 9c and 9d). These features generally agree with the distribution of relative residuals from all events (Figure 8).

[10] A 3-D grid was set up in the model to express the 3-D velocity structure. The model was parameterized with a grid spacing of 0.7° × 0.7° (∼70 km × 78 km) in map view and with grid nodes at depths of 1, 5, 15, 35, 70, 140, 210, 280, 350, 420, 500, and 580 km (Figure 6), after making many resolution tests with different grid intervals. Velocity perturbations at the grid nodes were taken as unknown parameters. We resolved 2758 velocity perturbations for the grid nodes with hit counts (number of rays passing near each grid node) larger than 10. A conjugate-gradient algorithm LSQR [*Paige and Saunders*, 1982] with damping and first-order smoothing regularizations [*Zhao*, 2001, 2004; *Lei and Zhao*, 2006a] was

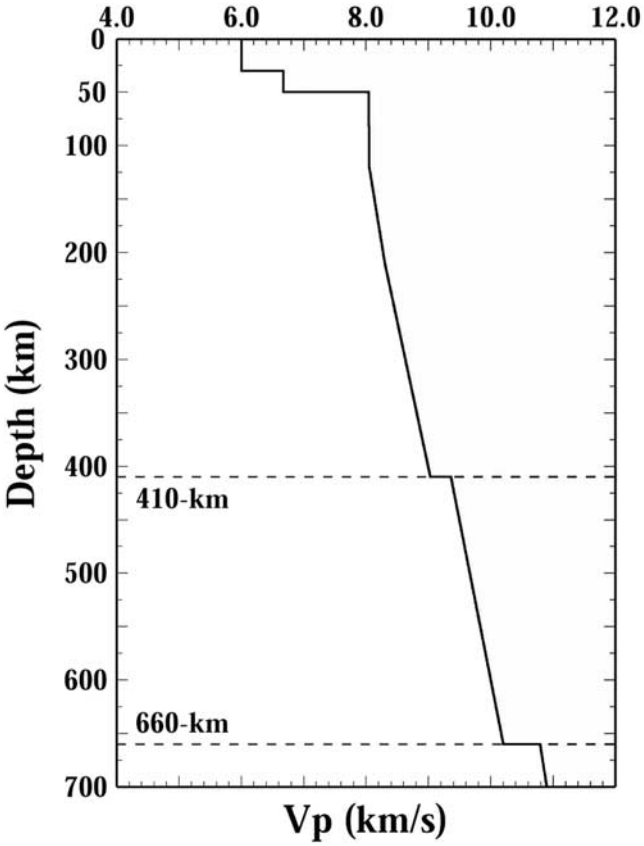


**Figure 4.** Starting 1-D velocity model used for the tomographic inversion in this study. This 1-D model was inferred from the previous studies [e.g., *Kan and Lin*, 1986; *Fan and Cheng*, 1992; *Xu et al.*, 2007] for the crust, and the International Association of Seismology and Physics of the Earth's Interior, 1991 (iasp91) model [*Kennett and Engdahl*, 1991] was adopted for the mantle. Two dashed lines denote the 410- and 660-km discontinuities.

used to resolve the large and sparse system of observational equations. By considering the balance between the reduction of traveltime residuals and the smoothness of the 3-D velocity model obtained [e.g., *Eberhart-Phillips*, 1986], the optimal value of the damping parameter is found to be 20.0 in the present study after performing many inversions with different values of the damping parameter.

## 3. Results and Resolution Analysis

[11] Figure 10 shows our resulting tomographic images in map view. A prominent low-V anomaly is visible under the Tengchong volcano from the surface down to about 420-km depth (Figures 10a–10j). Furthermore, this low-V anomaly forms a band from the northeast through the Tengchong volcanic field to the southeast in the crust and uppermost mantle (Figures 10a–10e). Between 280- and 350-km depth the low-V anomaly under the Tengchong volcano extends toward the east and northeast (Figures 10h and 10i), which may reflect the continuous dehydration of the northeastward moving Indian slab in the mantle transition zone. At 500- and 580-km depths, high-V anomalies are visible under the entire Yunnan Province except for some portions to the southeast of Tengchong (Figures 10k and 10l), possibly owing to the sparse ray coverage there (Figures 6k and 6l). Note that a prominent low-V anomaly matching well the orientation of the Red River fault is revealed at depths of 15–70 km (Figures 10c–10e), suggesting that the Red River fault may have cut through the Moho into the uppermost mantle. This result is different from that of *Wang and Burchfiel* [1997], who suggested the Red River fault to be a crustal-scale feature but consistent with that of *Leloup et al.* [1995], who suggested it to be a lithospheric-scale feature. The 2003 Dayao earthquakes occurred on the margin of high-V anomalies at 5- and 15-km depths (Figures 10b and 10c) and are underlain by an obvious low-V anomaly in the lower crust and upper mantle (Figures 10d and 10e). In addition, a very broad low-V anomaly in eastern Yunnan is revealed at 140- and 210-km depths (Figures 10f and 10g), indicating the existence of relatively hotter asthenospheric material there.

[12] In vertical cross sections, it can also be found that a prominent low-V anomaly under the Tengchong volcano extends down to about 400-km depth (Figures 11a–11c). Moreover, this low-V anomaly at depths of ~250–400 km extends toward the northeast (Figures 11b and 11c). Some high-V anomalies observed in the upper mantle may represent cold lithospheric material, while those in the mantle transition zone may denote the subducted Indian slab (Figures 11a–11c). The low-V zone under the Red River fault extends down to about 100-km depth (Figure 11b).

[13] In order to confirm the main features that appeared in the present results, we conducted many checkerboard resolution tests (Figures 11d–11f and 12), a restoring test

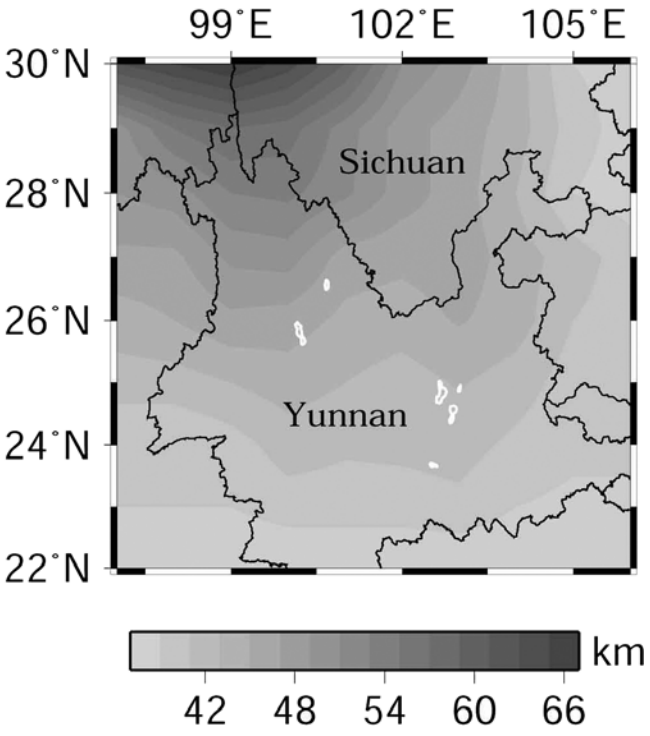


**Figure 5.** Illustration of the Moho discontinuity in the Yunnan and adjacent regions extracted from deep seismic soundings and receiver-function analyses [*Kan and Lin*, 1986; *Xu et al.*, 2007]. Depth scale (in km) is shown at the bottom.

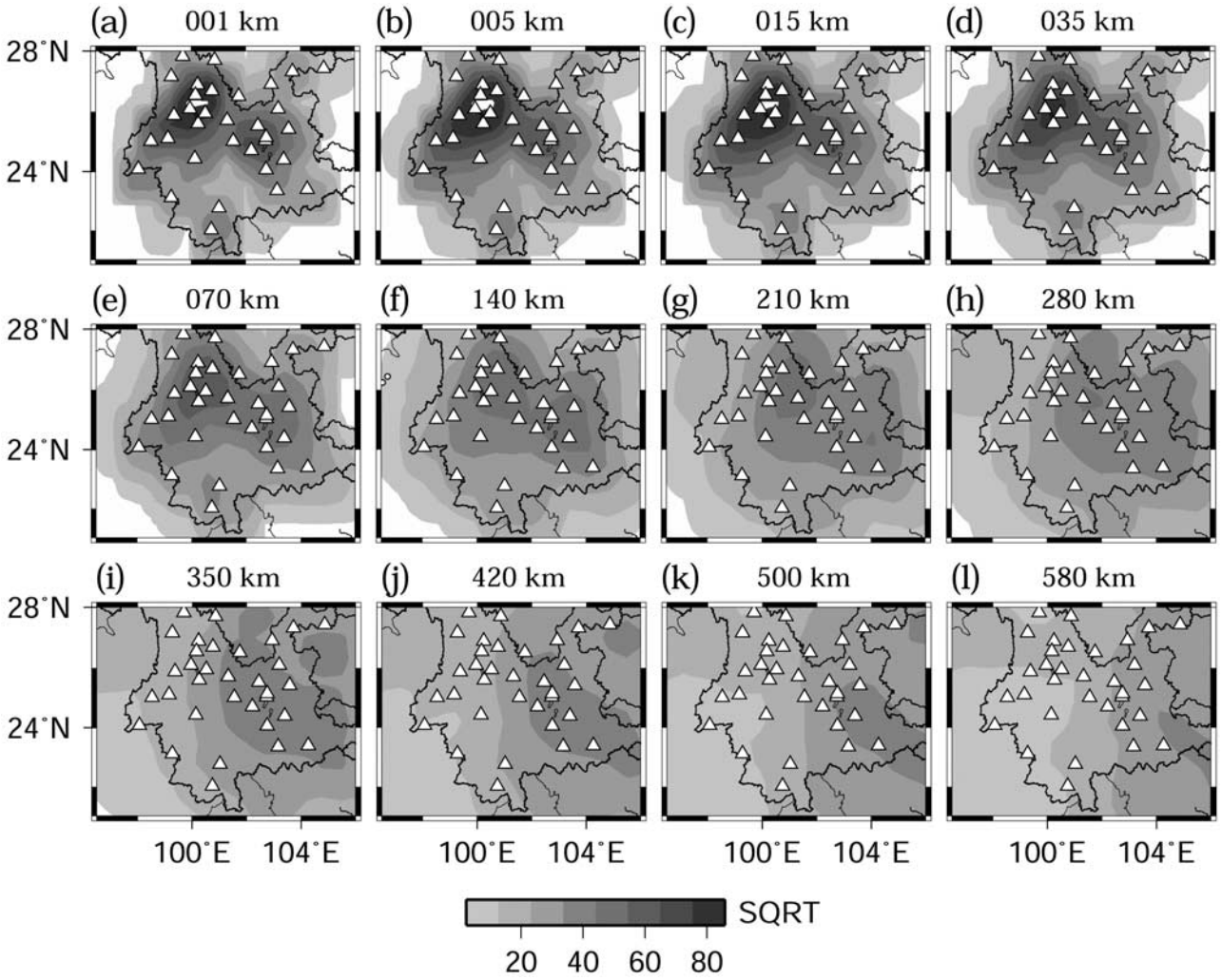


**Figure 6.** (a–l) Distribution of the number of the rays passing through each grid node (hit counts) in map view. The layer depth is shown above each map. The scale for the square root of the hit count is shown at the bottom. The triangles denote the seismic stations used in this study.

(Figures 11g–11i), and four synthetic tests (Figure 13) by applying the same algorithm and using the same numbers of stations, events and raypaths as those for the real inversion [see, e.g., *Humphreys and Clayton*, 1988; *D. Zhao et al.*, 1994, 2006; *Hung et al.*, 2004; *Lei and Zhao*, 2006b, 2007a]. Random errors having a normal distribution with zero mean and a standard deviation of 0.10 s were added to the synthetic travel times. In the checkerboard resolution test, positive and negative velocity perturbations of 2% relative to the 1-D velocity model as shown in Figure 4 are assigned to the 3-D grid nodes that are arranged in the modeling space. The resolution is much better in the middle and lower crust (Figures 12c and 12d) than in the upper crust (Figures 12a and 12b) because of the crisscrossing rays from teleseismic events and local earthquakes at those depths (Figures 3b and 3c). In the upper mantle the resolution becomes better with depth in the entire Yunnan Province (Figures 12e–12j), but in the mantle transition zone the well-resolved areas are biased toward the east with depth (Figures 12k and 12l). Such changes of the well-resolved areas with depth are closely associated with the distribution of seismic rays (Figure 3) and hit counts (Figure 6).

[14] In order to further affirm the seismic structure under Tengchong, we show the resolution along three vertical cross sections by using the star-cross way [*Lei and Zhou*, 2002]. Stars and crosses denote the grid nodes where the pattern of the input velocity anomalies is recovered correctly and wrongly after the inversion, respectively. The size of star and cross symbols denotes the ratio of the inverted amplitude of the velocity anomaly to that in the initial model. The stars with values of 100% show the grid nodes where the checkerboard model is recovered perfectly. In this expression, it is more straightforward to see where the resolution is good and where it is poor, particularly when a cross section does not pass right through the grid nodes. For details of this expression method, see the work of *Lei and Zhou* [2002] and *Lei and Zhao* [2005, 2007b]. The resolution is good along three vertical cross sections in the upper mantle and mantle transition zone, except for some places in the southern and western segments (Figures 11d–11f). In the restoring test, the input model is not alternating positive-negative anomalies but the 3-D velocity model (Figures 11a–11c) inferred from the real data. The procedure is the same as that used in the checkerboard resolution

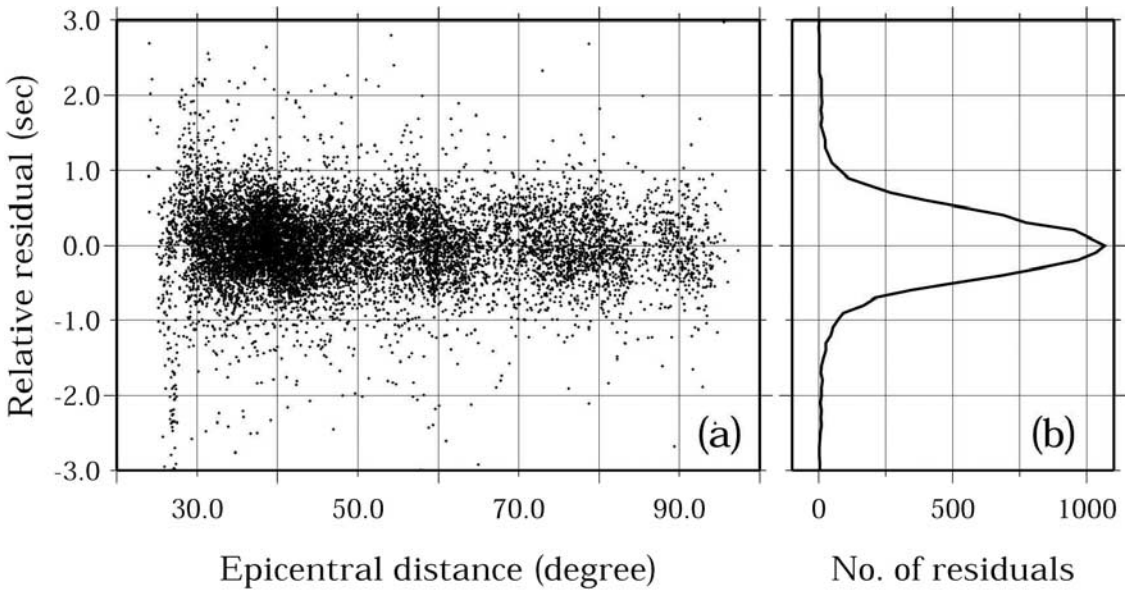


**Figure 7.** (a) Distribution of relative traveltime residuals in second versus epicentral distances in degrees. (b) Histogram of relative traveltime residuals. The number of residuals is added up within a range of 0.1 s and plotted in the center of the range.

test. The results of the restoring test (Figures 11g–11i) show that the pattern of velocity anomalies is well retrieved, though there are some minor differences in amplitude and geometry between the input and output models, suggesting that the main features revealed, such as low-V anomalies under the Tengchong volcano extending down to 400-km depth and high-V anomalies in the mantle transition zone, are reliable.

[15] To further confirm the reliability of the main features in the tomographic images obtained, we carried out a number of synthetic tests by changing the diameter and morphology of low- and high-V anomalies in the initial model. Among them, four synthetic tests are illustrated in Figure 13. In the first two tests we put low-V anomalies of up to −2% in the input model from the surface to 200- and 400-km depths, respectively (Figures 13a, 13b, 13e, and 13f). In the third test we put low-V anomalies of up to −2% extending northeastward above the mantle transition zone (Figures 13i and 13j). In the fourth test high-V anomalies of up to 2% are put in the mantle transition zone (Figures 13m and 13n). The output models (Figures 13c, 13d, 13g, 13h, 13k, 13l, 13o, and 13p) have a similar pattern as the input models, though some differences exist between them in amplitude and there is some smearing in the output models, particularly in the third and fourth tests (Figures 13i–13p). Nevertheless, these extensive resolution tests all suggest that the low-V anomaly under the Tengchong volcano extending down to about 400-km depth and then extending toward the northeast above the mantle transition zone and the high-V anomalies in the mantle transition zone are robust features.

## 4. Discussion

[16] The seismic structure of the crustal and upper mantle can be better constrained when both local and teleseismic data are used jointly [e.g., *Lei et al.*, 2009]. Therefore, in the present study we combined the local and teleseismic data to invert for the crustal and upper mantle heterogeneities under the Yunnan region. Our tomographic model provides new information on the intraplate Tengchong volcano and has

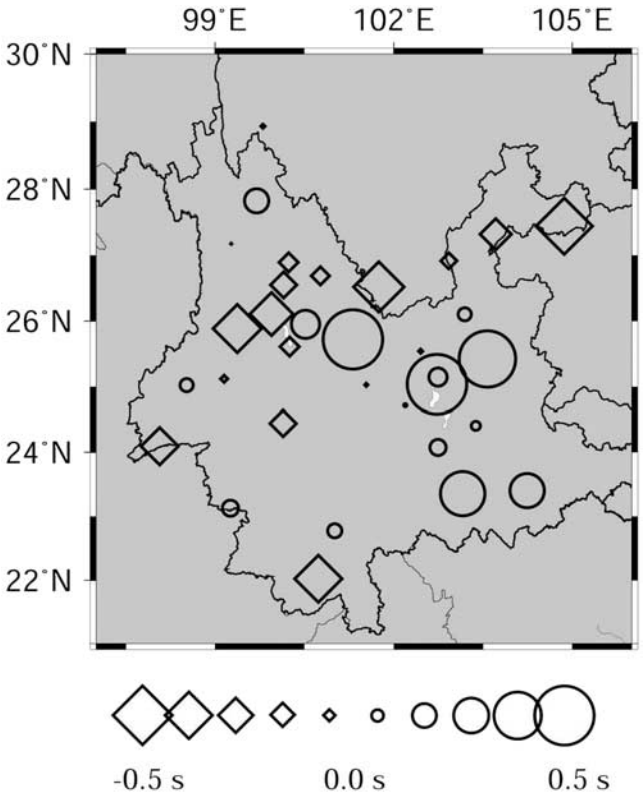


**Figure 8.** Distribution of relative traveltime residuals for all teleseismic events at every station. Diamonds and circles denote negative and positive residuals, respectively. The scale for the residuals (in seconds) is shown at the bottom.

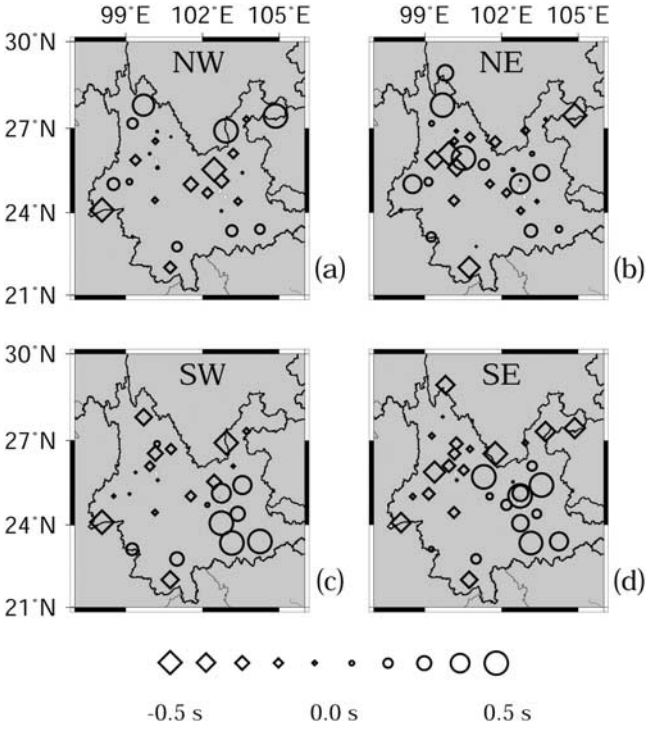


**Figure 9.** The same as Figure 8 but for four source quadrants: (a) northwest (NW, 270° < baz < 360°), (b) northeast (NE, 0° < baz < 90°), (c) southwest (SW, 180° < baz < 270°), and (d) southeast (SE, 90° < baz < 180°). baz, back azimuth from a seismic station to a teleseismic event.

revealed some velocity anomalies related to the Red River fault zone and the 2003 Dayao earthquakes.

### 4.1. Origin of the Tengchong Volcano

[17] Temperature measurements and geochemical analyses for many hot springs showed three areas with higher geothermal gradients in the Tengchong volcanic field, suggesting the existence of three magma chambers under the region [*C. Zhao et al.*, 2006]. The crust under Tengchong is characterized by low-*P* and low-*S* velocities through investigations of deep seismic soundings and teleseismic receiver functions [*Wang and Huangfu*, 2004], lower resistivity from magnetotelluric soundings [*Sun et al.*, 1989], high heat flow [*Wu et al.*, 1988], and low-Q values [*Qin et al.*, 1998]. *Huang et al.* [2002] revealed a low-V anomaly extending down to 85-km depth by using local-earthquake data. However, these studies did not resolve the depth range of the low-V anomaly under the Tengchong volcano. Global tomographic studies could not image clearly the low-V anomaly under the Tengchong volcano for understanding its origin because of their lower spatial resolution. Recent tomographic studies under East Asia showed a low-V anomaly down to 300-km depth under Tengchong, but the low-V zone has a lateral extent of ~500–600 km [*Huang and Zhao*, 2006], while *Li et al.* [2008a] illustrated a low-V anomaly under Tengchong extending down to only ~150-km depth. Our high-resolution tomographic model clearly shows a striking low-V anomaly of only ~150-km width under the Tengchong volcano extending down to about 400-km depth (Figures 10 and 11a–11c). Another significant feature of our present model is that the low-V anomaly at ~250- to 400-km depths under Tengchong extends horizontally toward the northeast (Figures 11b and 11c), which may suggest that the dehydration reaction continues when the subducted Indian slab in the mantle transition zone moves toward the northeast because the low-V anomaly at ~250- to 400-km depths exists right above the high-V anomalies in the mantle transition zone (Figures 11b and 11c).

[18] Previous studies showed significant discrepancies in the depth range of the subducted lithosphere in the region. *Wang and Huangfu* [2004] suggested that the subducted plate extends down to ~200-km depth right under the Tengchong volcano, while *Huang and Zhao* [2006] proposed that the plate could have subducted down to 400-km depth under Tengchong. In the present study high-V anomalies are observed in the mantle transition zone under Tengchong (Figures 10 and 11a–11c), which may represent cold material of the subducted lithosphere. This interpretation is supported by recent tomographic results [*Li et al.*, 2008a] as well as isotopic and geochemical studies [*Zhu et al.*, 1983]. Our extensive resolution tests (Figures 11d–11i, 12, and 13) show that the main features of the present result are reliable. The use of a large number of high-quality arrival time data recorded by the dense Yunnan seismic network has resulted in the present high-resolution tomographic model.

[19] Geochemical arguments and regional structural correlations suggested that the early igneous phase (42–24 Ma) was generated by continental subduction [e.g., *Wang et al.*, 2001], while in the later episode (16–0 Ma) the Tengchong volcanic rocks are considered to be rift-related [e.g., *Yin*, 2000; *Wang et al.*, 2001]. Although geophysicists cannot rule out this possibility, all geophysical results so far suggested that the origin of the Tengchong volcano is related to the plate subduction [e.g., *Zhu et al.*, 1983; *Wang and Huangfu*, 2004; *Huang and Zhao*, 2006; *Hu et al.*, 2008; *Li et al.*, 2008a]. Therefore, we conclude that the formation of the Tengchong volcano is not only related to the subduction of the Indian plate, but also controlled by the rifting process (Figure 1a). The present tomographic model does not cover the areas west of Yunnan. The hypocentral distribution of intermediate-depth earthquakes defines a clear Wadati-Benioff zone down to ~180-km depth [*Engdahl et al.*, 1998] (Figure 1b), but this feature is visible only west of the Myityina-Mandalay fault that is ~120 km west of the Tengchong volcanic field (Figure 1). Integrating the upper mantle image west of the Tengchong volcano by *Huang and Zhao* [2006] and *Li et al.* [2008a], we infer that the high-V anomalies in the mantle transition zone revealed by our model (Figures 10 and 11a–11c) may represent the subducted Indian plate. A prominent low-V anomaly is visible down to 400-km depth right beneath the Tengchong volcano and it overlies high-V anomalies in the mantle transition zone. Such a structure is different from that under the Hainan hot spot volcano in southernmost China where a low-V anomaly ascends from the lower mantle [e.g., *Lebedev et al.*, 2000; *Montelli et al.*, 2004; *Lei et al.*, 2009], but it is quite similar to that under the Changbai volcano in northeast China where a prominent low-V anomaly extends down to 400-km depth and the Pacific slab is stagnant in the mantle transition zone [*Lei and Zhao*, 2005]. Therefore,

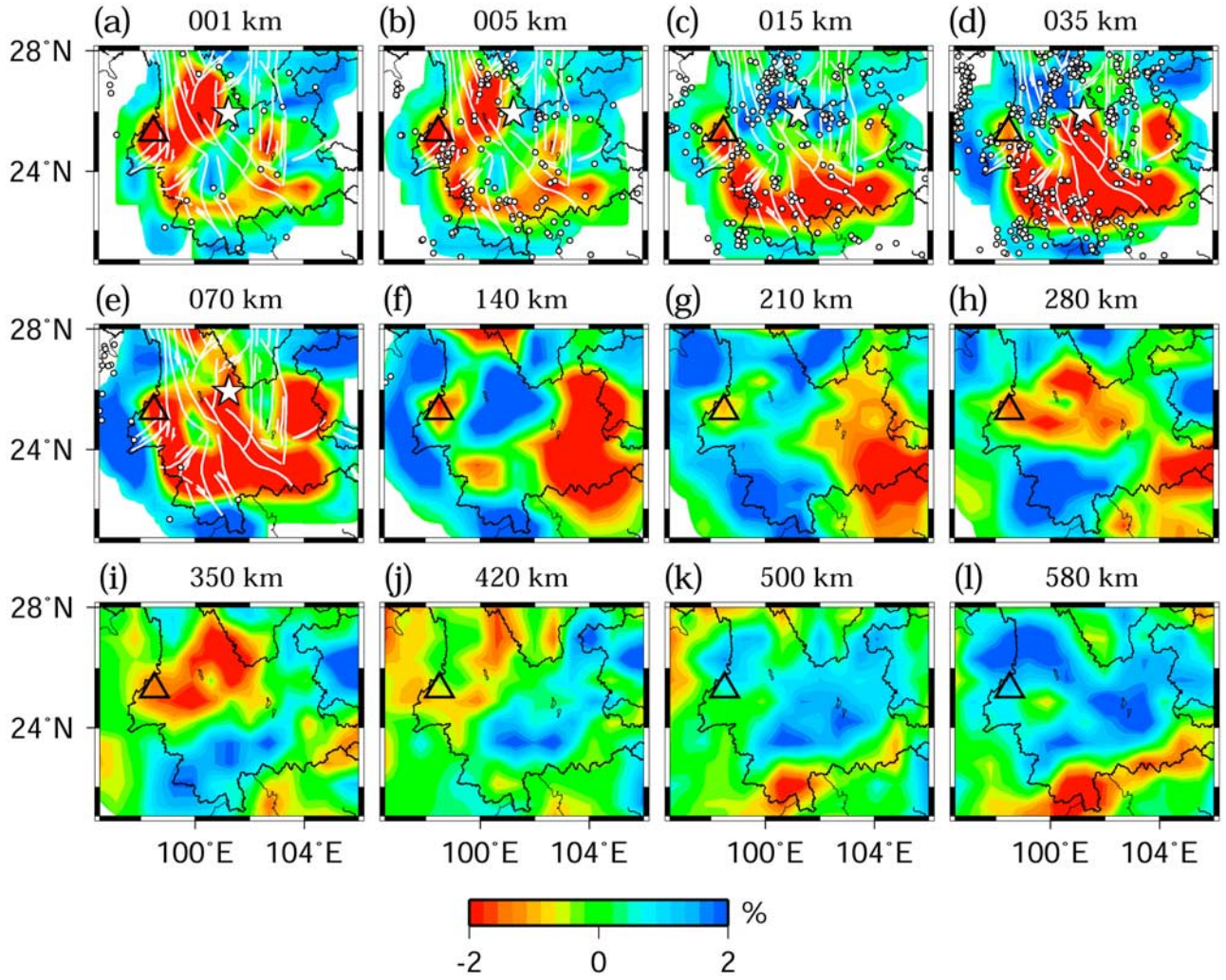


**Figure 10.** (a–l) Obtained tomographic images in map view, relative to a 1-D velocity model as shown in Figure 4. Red and blue colors denote low- and high-velocity anomalies, respectively. The color scale for the velocity perturbation (in %) is shown at the bottom. The layer depth is shown above each map. Open triangles denote the Tengchong volcano. Two white stars (quite close, ~8-km separation) in Figures 10a–10e represent the 21 July 2003 Dayao earthquake (*M* 6.2) and the 16 October 2003 Dayao earthquake (*M* 6.1) [*Hua et al.*, 2006], respectively. White lines in Figures 10a–10e denote major active faults. White dots in Figures 10a–10f denote earthquakes during 1964–2004 [*Engdahl et al.*, 1998] within half distances between two neighboring layers.

**Figure 11.** (a–c) Same as Figure 10 but for three vertical cross sections as shown on the inset map. Red and blue colors denote slow and fast anomalies, respectively. The scale for the velocity perturbation (in %) is shown on the right of Figure 11c. The topography profile is shown at the top. Red triangles in Figures 11a–11i denote the Tengchong volcano. Inverted triangles in Figures 11b, 11e, and 11h denote the Red River fault zone. Dashed lines in Figures 11a–11i denote the Moho, 410-, and 660-km discontinuities. White dots in Figures 11a–11c denote earthquakes in a range of 35 km off each profile. These earthquakes, relocated by *Engdahl et al.* [1998], have magnitude 3 or greater and occurred during 1964–2004. Locations of the cross sections are shown on the inset map, where white triangles denote the seismic stations used. (d–f) Result of a checkerboard resolution test along the corresponding cross sections. Stars and crosses denote the grid nodes where the pattern of the input velocity anomalies is recovered correctly and wrongly after the inversion, respectively. The size of star and cross symbols denotes the ratio of the inverted amplitude of the velocity anomaly to that in the initial model. For details, see the text. (g–i) Result of a restoring test. In this test, we took the model of Figures 11a–11c inferred from the real data set as the input model, which is only different from the checkerboard resolution test [*Zhao et al.*, 1994; *C. Zhao et al.*, 2006; *Hung et al.*, 2004; *Lei and Zhao*, 2006b, 2007a]. The symbols are the same as those shown in Figures 11a–11c. There is no vertical exaggeration except for surface topography on the top of Figures 11a–11c.

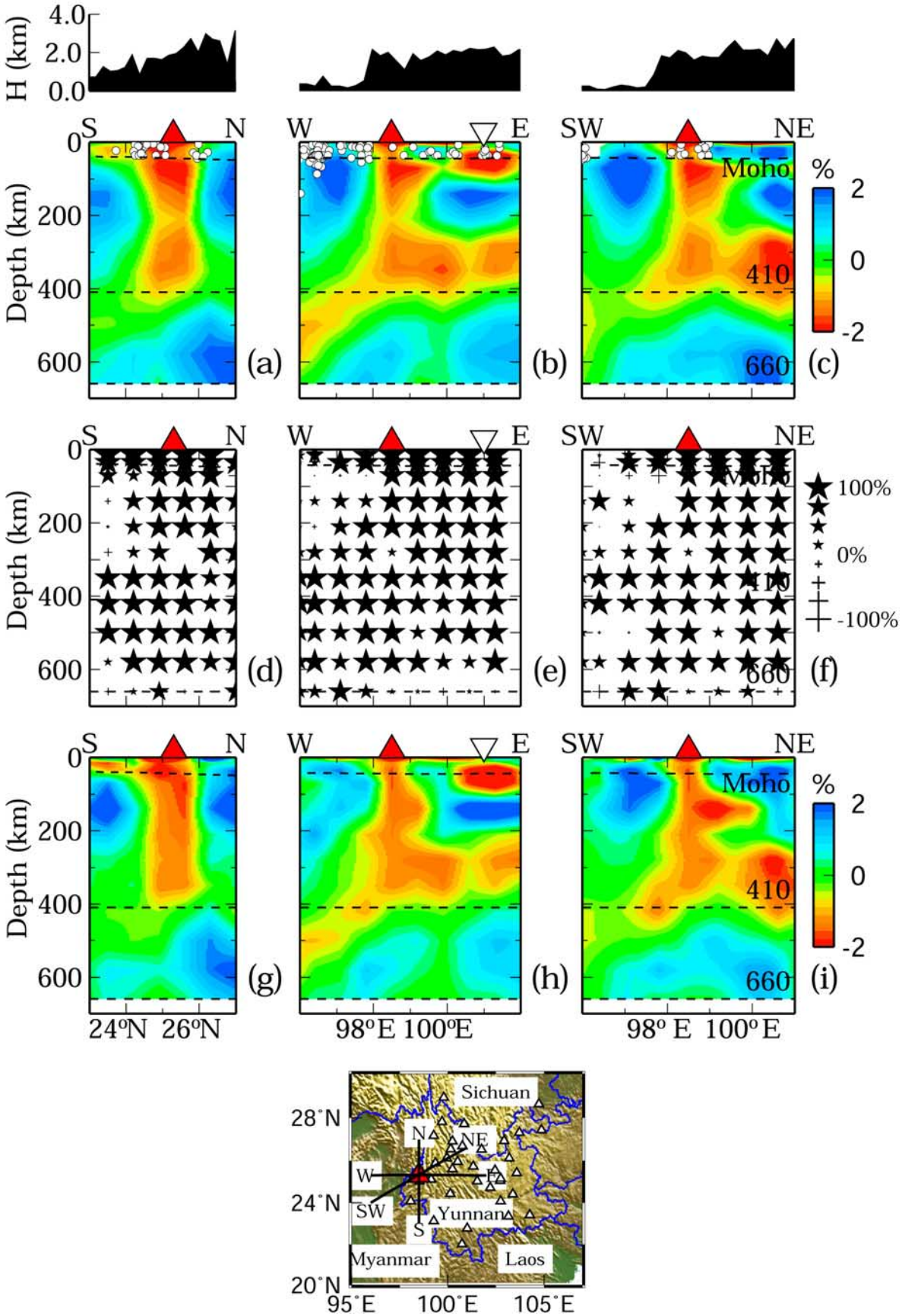
H (km)
4.0
2.0
0.0
S
N
W
E
SW
NE
Depth (km)
0
200
400
600
Moho
410
660
%
2
0
-2
(a)
(b)
(c)
100%
0%
-100%
(d)
(e)
(f)
(g)
(h)
(i)
24°N 26°N
98°E 100°E
Sichuan
Yunnan
Myanmar
Laos
28°N
24°N
20°N
95°E
100°E
105°E

**Figure 11**

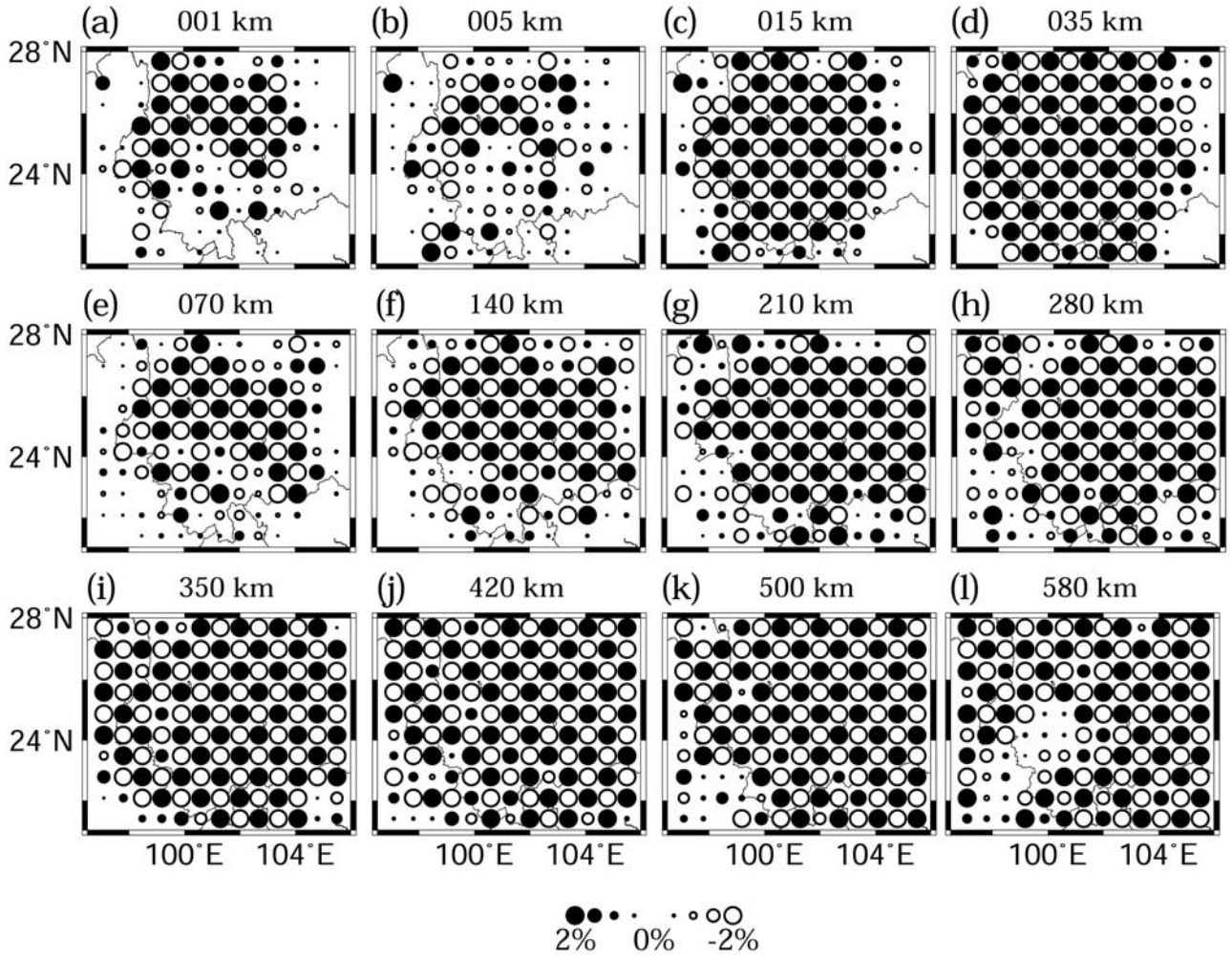


**Figure 12.** (a–l) Results of a checkerboard resolution test for *P* wave structure in map view. The model has been parameterized with a grid spacing of 0.7° × 0.7° (~70 km × 78 km) in the horizontal direction. The layer depth is shown above each map. White and black dots denote the slow and fast velocity anomalies, respectively. The scale for the velocity perturbation (in %) relative to the 1-D velocity model mentioned in section 2 is shown at the bottom.

following the interpretation of *Huang and Zhao* [2006], *Yin* [2000], and *Wang et al.* [2001], the Tengchong volcano can be regarded as a subduction-zone volcano which is rift-related and caused by the slab dehydration and corner flow in the mantle wedge, though the subducted slab is a continental plate. However, our results suggest that the upwelling flow under Tengchong may originate at about 400-km depth (Figures 11a–11c), which have significantly improved over previous studies and provide new constraints on the dynamic process of the India-Asia collision. Further efforts should be made to deploy portable seismic stations in Myanmar to determine a detailed seismic structure from Myanmar to Yunnan to clarify the origin of this significant intraplate volcano.

### 4.2. Deep Structure of the Red River Fault Zone

[20] The Red River fault zone is an over 1000 km long strike-slip fault, which begins at the eastern portion of the Tibetan Plateau and northwestern portion of Yunnan, passes through northern Vietnam, and extends eastward into the South China Sea [e.g., *Zhong et al.*, 1989; *Tapponnier et al.*, 1990; *Lee and Lawver*, 1995; *Leloup et al.*, 1995] (Figure 1). The continent-continent collision of the Indian plate with the Eurasian plate caused the uplift of the Tibetan Plateau and the southeastward rotating extrusion of the Indochina block [*Tapponnier et al.*, 1990; *Scharer et al.*, 1990], so the Red River fault zone is regarded as a major tectonic boundary between the south China and Indochina blocks [*Scharer et al.*, 1994; *Leloup et al.*, 1995]. It is suggested that the tectonic evolution of the Red River fault zone includes two stages of the sinistral slip during the Tertiary and the dextral slip in the Quaternary [*Scharer et al.*, 1990]. Hence, studying the deep structure of the Red River fault zone is of great importance for understanding the collision of the Indian and the Eurasian plates.

[21] Different researchers illustrated various geometries of velocity anomalies along this fault zone. In the upper and middle crust, some results show that the Red River fault zone is an obvious high-V anomaly interpreted as the rising and rapid cooling of the metamorphic rocks after the ductile

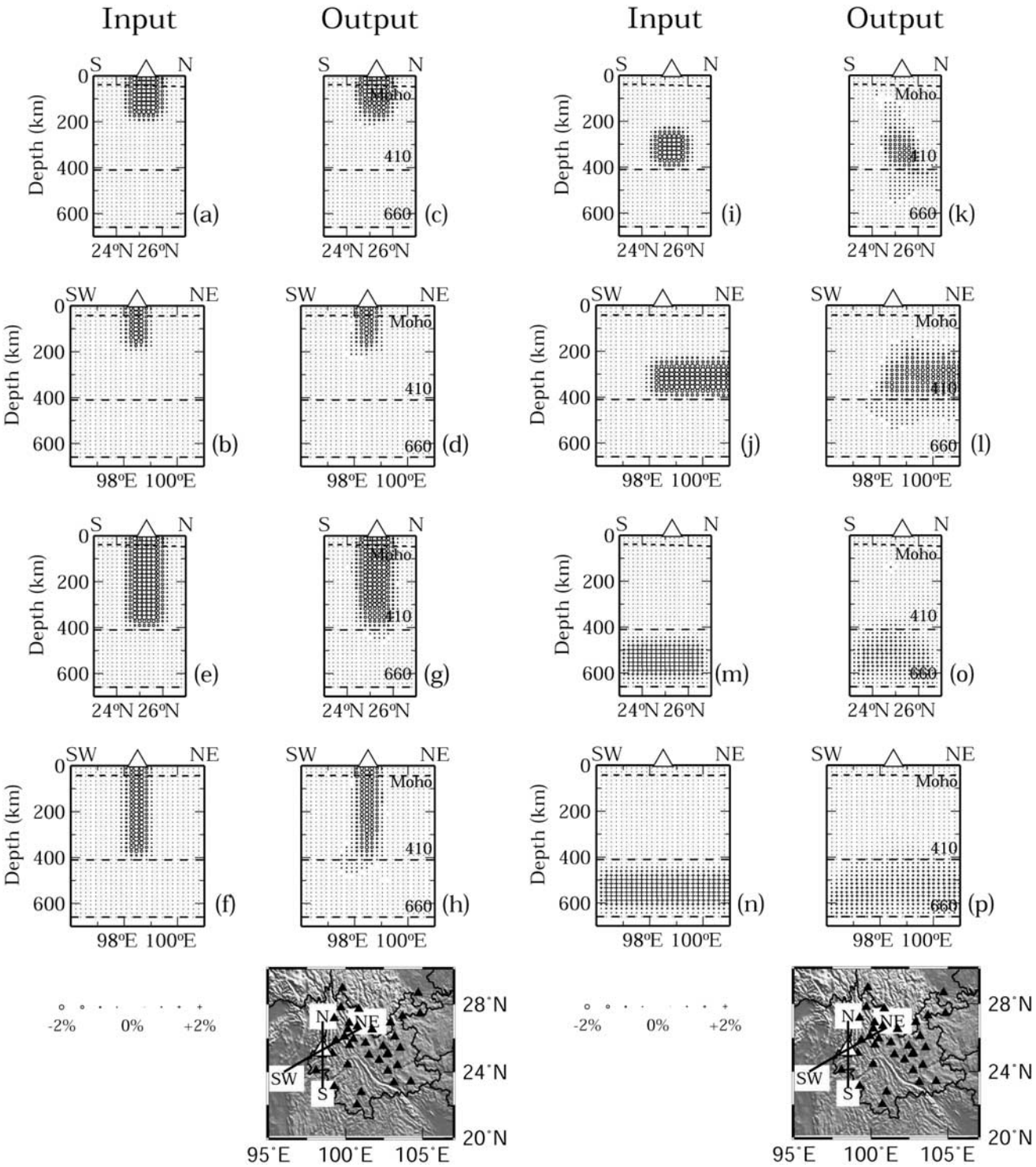


**Figure 13.** (a–p) Four synthetic tests. Figures 13a, 13b, 13e, 13f, 13i, 13j, 13m, and 13n show input models, and Figures 13c, 13d, 13g, 13h, 13k, 13l, 13o, and 13p show output models. Circles and crosses denote slow and fast velocity anomalies. The velocity perturbation scale (in %) is shown at the bottom. Dashed lines denote the Moho, 410-, and 660-km discontinuities. Locations of cross sections are shown on the inset map. White triangles denote the Tengchong volcano, while black triangles denote the seismic stations used in this study.

shearing [e.g., *Xu et al.*, 2003], while others illustrated a transition zone from positive anomalies in the northeastern region of the Red River fault to negative anomalies in the southwestern region [e.g., *Huang et al.*, 2002; *Wang et al.*, 2003]. In the lower crust, the models of *Huang et al.* [2002], *Wang et al.* [2003], and *Li et al.* [2008b] show that the Red River fault zone is still a boundary between low- and high-V anomalies, while our model shows a prominent low-V

anomaly under the Red River fault zone (Figure 10d), which is in agreement with previous tomographic studies [e.g., *Xu et al.*, 2003] and receiver-function analyses [*Xu et al.*, 2005]. In the upper mantle, the models of *Xu et al.* [2003] and *Li et al.* [2008b] display a boundary of low- and high-V anomalies along the Red River fault, while our model illustrates a prominent low-V anomaly along the fault (Figure 10e), which is consistent with the result of *Wang et al.* [2003]. Recent surface-wave tomography revealed prominent low-V anomalies along the Red River fault in the upper crust, but this feature seems to disappear in greater depth [e.g., *Yao et al.*, 2006, 2008]. These differences may be due to the different data sets and techniques used. Another possibility is that in our present work a number of high-quality local and teleseismic arrival times are picked only from digital seismic waveforms, which is different from some previous studies utilizing arrival data from analog recordings. However, our present results display a clear low-V zone of up to −5% along the Red River fault zone in the lower crust and upper mantle (down to ∼100-km depth) (Figures 10c–10e and 11b), quite consistent with recent tomographic studies [e.g., *Li et al.*, 2008a], indicating that the Red River fault zone has been cut through the crust, reaching down to the upper mantle. The result is different from that of *Wang and Burchfiel* [1997], who considered it to be a crustal-scale fault, but consistent with that of *Kan and Lin* [1986] and *Leloup et al.* [1995], who suggested that it may be a lithospheric-scale feature. Such a velocity structure along the Red River fault zone (Figures 10c–11e and 11b) has been demonstrated to be a robust feature by extensive resolution tests (Figures 11 and 12). This result supports the proposal that the Red River fault zone is a channel for the rising of hot material toward the crust from the mantle [e.g., *Xu et al.*, 2003].

[22] Several other major fault zones also exist in Yunnan Province, China, such as the Nujiang, Lancang River, and Xiaojiang fault zones (Figure 1a). These fault zones correspond to velocity anomalies extending down to various depths. For example, along the Nujiang fault zone the low-V anomaly only extends down to 5-km depth (Figures 10a and 10b), while in the southern portion of the Lancang River fault zone it extends down to the upper mantle (Figures 10a–10e). The Xiaojiang fault zone is located at the edge of a low-V anomaly from the crust to the upper mantle (Figures 10a–10e). For more details of the deep structure of these fault zones, the deployment of more seismic stations would be required, in order to improve the raypath coverage across the fault zones.

### 4.3. Mechanism of the 2003 Dayao Earthquakes

[23] In the Yunnan region strong earthquakes occur frequently, and there are numerous small earthquakes ($M < 5.0$) [*Engdahl et al.*, 1998]. Over 150 earthquakes with $M$ 5.0–6.0, and more than 35 strong crustal earthquakes with $M \geq 6.0$ occurred since 1970, 8 of which were larger than $M$ 7.0, such as the 1970 Tonghai earthquake ($M$ 7.8), the 1976 Longling earthquake ($M$ 7.4), the 1988 Lancang earthquake ($M$ 7.4) and the 1996 Lijiang earthquake ($M$ 7.0) (Figure 1a) (China Earthquake Administration, unpublished catalogue of China strong earthquakes, 2005). After a 632-day quiescence of the earthquakes with $M$ 5.0 or larger in the Yunnan region following the 27 October 2001 Yongsheng earthquake ($M$ 6.0), two earthquakes successively occurred on 21 July and 16 October 2003 in the Dayao region, which caused 19 deaths and over 600 people to be injured, and extensive property losses [*Su*, 2004; *He et al.*, 2005]. Their focal depths are accurately redetermined by *Hua et al.* [2006] to be 11.8 and 9.2 km, respectively (Figure 14) by applying the double-difference location method of *Waldhauser and Ellsworth* [2000]. The uncertainties of the two focal depths are 0.20 and 0.26 km, respectively [*Hua et al.*, 2006]. It is generally accepted that in the Yunnan region, most earthquakes larger than $M$ 6.0 occurred along major active tectonic or seismic zones [e.g., *Deng et al.*, 2002], but the 2003 Dayao earthquakes are located within the interior of the Dian-Zhong block (Figure 1a), where there are no obvious surface expressions of fault zones [*Su*, 2004]. However, the hypocentral locations of these two main shocks and the preferred trending of their aftershocks strongly suggested the existence of a NWW oriented fault zone in the source area [*Hua et al.*, 2006], which was also demonstrated by the velocity and Q structures in the source areas [*Wang et al.*, 2007]. Because the NWW oriented Chouxiong-Nanhua fault zone is close to the 2003 Dayao earthquakes (Figure 1a) [*Deng et al.*, 2002; *Su*, 2004], some researchers suggested that the two earthquakes were caused by the northward rupturing of the Chouxiong-Nanhua fault zone since the 2000 Yao-An earthquake ($M$ 6.5) [e.g., *He et al.*, 2005].

[24] Previous studies have investigated the causes of the strong crustal earthquakes in the region, and found that most of them in the region occurred at the boundary between low- and high-V anomalies [e.g., *Huang et al.*, 2002; *Wang et al.*, 2003]. Here, we mainly focus on the causes of the 2003 Dayao earthquakes. It can be clearly seen that the two Dayao earthquakes occurred at the boundary of low- and high-V anomalies and near high-V anomalies (Figures 10a–10e and 14). A recent tomographic study also found that the 28 July 1976 Tangshan earthquake ($M$ 7.8) in east China occurred at the edges of high-V anomalies along the Tangshan-Ninghe fault zone [e.g., *Lei et al.*, 2008]. *Wang and Zhao* [2006] found that the 2005 Fukuoka earthquake ($M$ 7.0) in southwest Japan was located near the high-V anomalies within the fault zone. *Hauksson and Haase* [1997] also revealed that four $M > 5.9$ earthquakes in the Los Angeles basin occurred in and adjacent to high-V anomalies along the faults. These results suggested that there are strong heterogeneities within the fault zones and the mechanical strength of materials located at the edge of high-V anomalies is higher than that of the low-V anomaly areas but still weaker than normal sections of the seismogenic layer. Hence the margin of a high-V anomaly is an ideal place to generate a large crustal earthquake.

[25] Figures 14e and 14f shows the absolute velocity maps along the vertical cross sections N-S and W-E. In some cases the variation extent of velocities is not easily judged quantitatively, and the gradient map is considered to be an efficient way to highlight a transition from high- to low-V anomalies (Figures 14c and 14d) [*Fishwick*, 2006]. It can also be seen that the Dayao earthquakes occurred at the edges of the high- and low-V anomalies but near the high-V anomalies in the cross section W-E (Figures 14b and 14f), hence the gradient there is relatively smaller (Figure 14d), but the cross section N-S clearly shows that the Dayao earthquakes occurred around a high-gradient zone (Figure 14c).

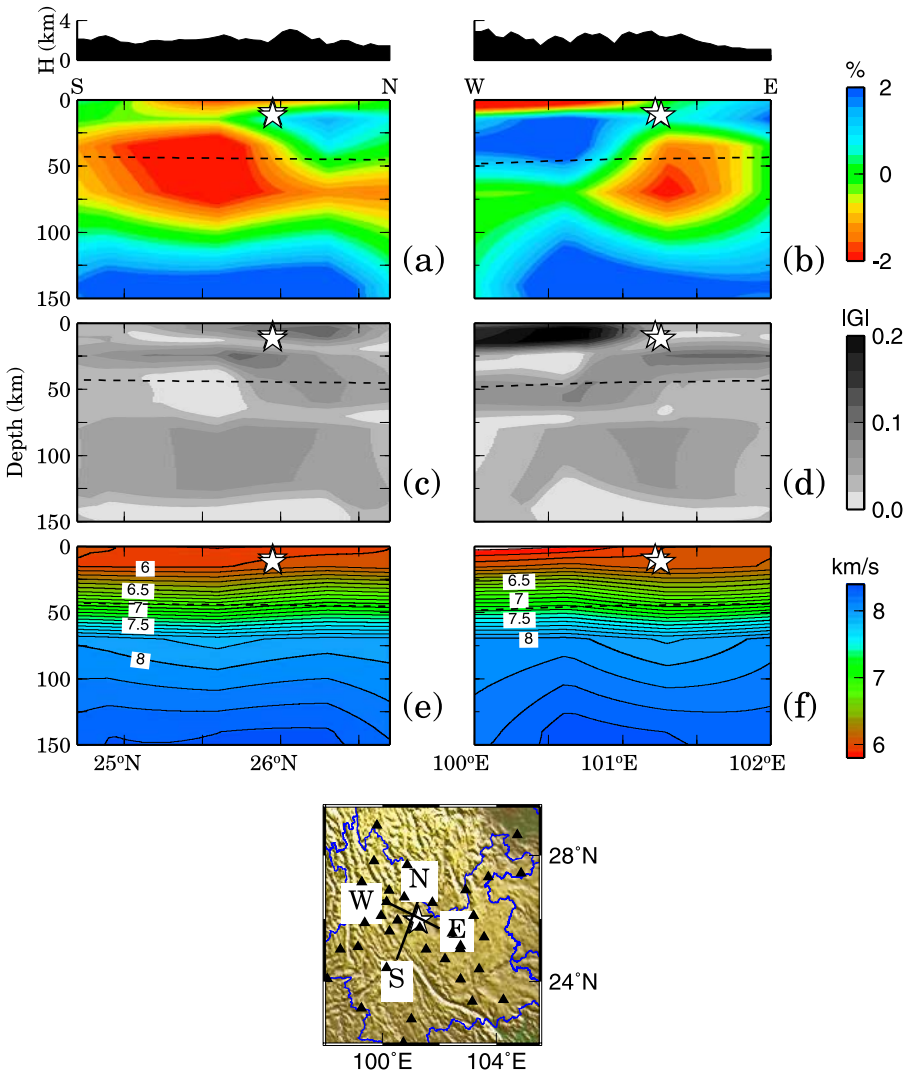


**Figure 14.** (a, b) Velocity perturbations along the vertical cross sections N-S and W-E passing through the 2003 Dayao earthquakes (stars). Red and blue colors denote slow and fast velocity anomalies. The scale for velocity perturbations is shown on the right of Figure 14b. The topography is plotted at the top of each cross section. The location of the cross sections is shown as black lines on the inset. Black triangles in the inset denote the seismic stations used in this study. The dashed line denotes the Moho discontinuity. (c, d) The magnitude of the velocity perturbation gradient calculated by applying the finite difference approximation [*Fishwick*, 2006] to the velocity perturbations as shown in Figures 14a and 14b. (e, f) Same as Figures 14a and 14b but for the absolute velocity. The symbols in Figures 14c–14f are the same as those in Figures 14a and 14b.

[26] Although geochemical studies suggested no participation of fluids in the genesis of the Tengchong volcanic rocks because they lack a Nb and Ta anomaly [e.g., *Wang et al.*, 2001], many geophysical studies have revealed the wide existence of fluids in the crust and uppermost mantle in subduction zones [e.g., *Tatsumi*, 1989; *Peacock*, 1990; *Iwamori*, 1998; *Zhao et al.*, 2002]. The Yunnan region is located in the region of the Indian plate subduction, as discussed in section 4.1 and in previous studies [e.g., *Huang and Zhao*, 2006; *Wang and Huangfu*, 2004]. Our present results show that the Dayao earthquakes are underlain by a prominent low-V zone (Figures 10a–10e and 14), being consistent with previous results for the crust inferred only from local-earthquake arrival time data [e.g., *Hua et al.*, 2006; *Zhou et al.*, 2007]. This is quite similar to the velocity structural features in regions near other large crustal earthquakes in Yunnan, as revealed by previous work [e.g., *Huang et al.*, 2002]. Furthermore, our results, obtained by adding the teleseismic data, clearly display a low-V anomaly extending down to the upper mantle (Figures 10a–10e and 14). These low-V anomalies may be closely associated with fluid-filled fractured rocks. Deep fluids may be liberated through the slab dehydration, if the high-V anomalies in the mantle transition zone (Figures 10k, 10l, and 11a–11c) represent the subducted Indian slab, as discussed in section 4.1. Fluids in and below the seismogenic layer may affect the long-term structural and compositional evolution of the fault zone, change the fault zone strength, and alter the local stress

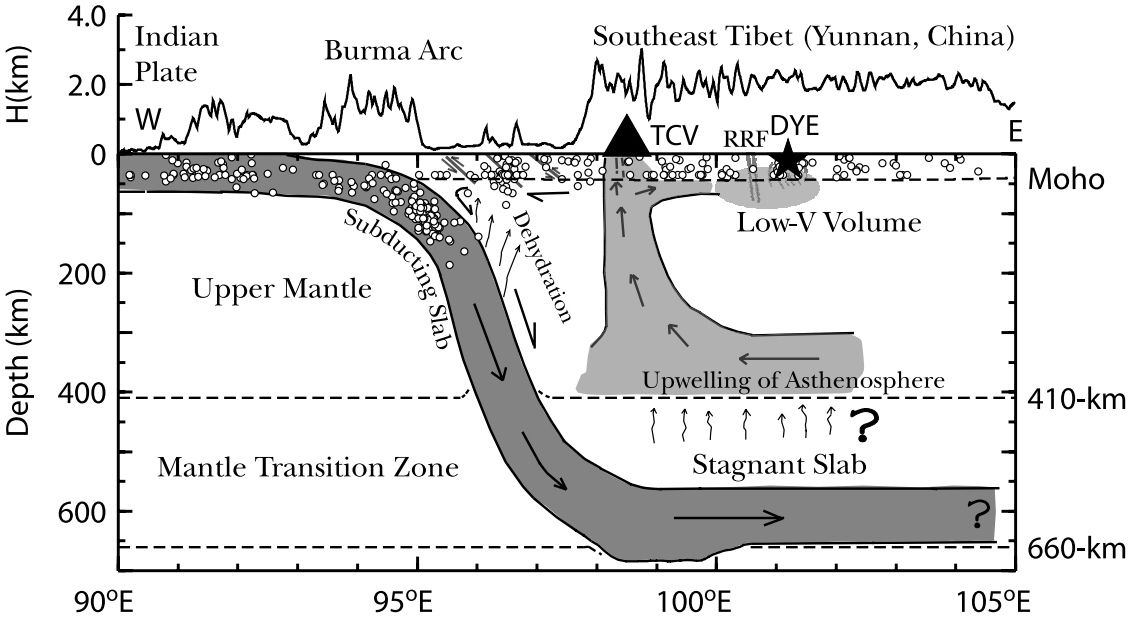


**Figure 15.** A schematic west-east vertical cross section showing the upper mantle structure under the Indian plate, Burma Arc, and southeast Tibet (Yunnan, SW China). See text for details. The triangle shows the Tengchong intraplate volcano (TCV). Stars represent the 2003 Dayao earthquakes (DYE). Thick double lines denote the Red River fault (RRF). Thin curves under the stars denote the fractured fault zones. Small white dots denote the earthquakes (1964–2004, $M > 3.0$, reprocessed by *Engdahl et al.* [1998]) that occurred within the 35 km of the profile along the latitude 25.3°N, as shown in Figure 1a. The curve at top shows the topography along the profile. There is no vertical exaggeration except for surface topography on the top.

regime [*Sibson*, 1982, 1992; *Hickman et al.*, 1995]. Owing to the fluid pressure and a variety of chemical effects, stress concentration is enhanced in the seismogenic layer resulting in the mechanical failure of a strong asperity [*Zhao et al.*, 2004]. These factors may make a significant contribution to the nucleation processes of the 2003 Dayao earthquakes. These processes are somewhat similar to those that caused the 1995 Kobe, Japan, earthquake [*Zhao et al.*, 1996], the 2001 Bhuj, India, earthquake [*Mishra and Zhao*, 2003], and the 1976 Tangshan, China, earthquake [e.g., *Lei et al.*, 2008]. Our study provides a new piece of evidence for the presence of fluids in the source area of the 2003 Dayao earthquakes, which may improve our understanding of the genesis of damaging earthquakes in the Yunnan region.

### 4.4. Interpretation

[27] The Tengchong volcano has been inferred to be related to the subduction of the Indian plate down to only ~200-km depth with a small dip angle of ~30° [*Wang and Huangfu*, 2004]. *Huang and Zhao* [2006] revealed high-V anomalies related to the subducted Indian slab above the mantle transition zone and low-V anomalies associated with the Tengchong volcano above 300-km depth. *Li et al.* [2008a] illustrated high-V anomalies related to the subducted Indian slab down to the mantle transition zone with a big dip angle of ~60° below ~200-km depth (in the aseismic zone) and low-V anomalies associated to the Tengchong volcano just above ~150-km depth. Recent receiver function analyses demonstrated that the 660-km discontinuity is depressed to 690-km depth under the Tengchong station [e.g., *Shen et al.*, 2008]. Our present tomographic model clearly shows high-V anomalies in the mantle transition zone and low-V anomalies under the Tengchong volcano extending down to ~400-km depth and further extending northeastward (Figures 10 and 11a–11c).

[28] Combining our present results with previous work [e.g., *Wang and Huangfu*, 2004; *Huang and Zhao*, 2006; *Li et al.*, 2008a; *Shen et al.*, 2008], we propose a model (Figure 15) of the upper mantle structure under the Indian plate, Burma Arc, and Southeast Tibetan Plateau (Yunnan, southwest China) to explain the origin of the Tengchong intraplate volcano as well as seismotectonics in the region. Such a tectonic model is somewhat similar to that explaining the origin of the Changbai intraplate volcano in northeast China [*Lei and Zhao*, 2005]. A difference between these two models is that the present model illustrates an obvious low-V layer more than 100 km thick extending northeastward above the mantle transition zone, which may suggest the continuous dehydration of the slab while moving northeastward in the mantle transition zone. In our model proposed, the Indian slab has subducted down to the mantle transition zone though the seismicity within the slab ends at ~200-km depth, and the dip angle of the slab varies from ~30° above ~200-km depth (in the seismic zone) to ~60° below ~200-km depth (in the aseismic zone) (Figure 15), which are quite similar to those observed in the subducted Philippine Sea slab [*Abdelwahed and Zhao*, 2007].

[29] Hot asthenospheric material in the deeper mantle and fluids released from the dehydration of the subducted Indian slab in the mantle transition zone may cause an upwelling in the upper mantle that reaches the surface along the rift zones

[e.g., *Yin*, 2000; *Wang et al.*, 2001], leading to the formation of the Tengchong volcano (Figure 15). We conclude that the formation of the Tengchong volcano is not only related to the subduction and dehydration of the Indian slab, but also associated with the distribution of the rift zones. When the hot and wet material reaches the uppermost mantle, it also flows in the horizontal directions. When the hot material with fluids arrived under the Red River fault, it may intrude upward along the broken section of the fault (Figure 15), which provides a channel for the rising of hot material from the upper mantle [e.g., *Xu et al.*, 2003]. This may explain the low-V anomalies down to the upper mantle along the Red River fault (Figures 10 and 11a–11c). When hot and wet material reached the source areas of the 2003 Dayao earthquakes, fluids may have entered the fractured fault zone and decreased the friction of the fault, leading to failure of a strong asperity [*Zhao et al.*, 2004] and triggering of the Dayao earthquakes. The low-V anomalies under the source areas in the lower crust and uppermost mantle may represent fluid-filled fractured rocks (Figures 14a, 14b, and 15).

## 5. Conclusions

[30] A high-resolution tomographic model of the crust and upper mantle under the Chinese Yunnan Province has, for the first time, been obtained by using a large number of high-quality teleseismic data and local-earthquake arrival times recorded by the dense Yunnan seismic network. Our present results provide new insights into the origin of the Tengchong volcano. A prominent low-V anomaly under Tengchong extends down to about 400-km depth, and high-V anomalies exist in the mantle transition zone. Integrating our tomographic images with geochemical and geological results, we conclude that the Tengchong volcano is a rift-related volcano caused by the subduction and dehydration of the Indian plate and corner flow in the mantle wedge.

[31] The Red River fault zone is imaged as a low-V anomaly extending down to the upper mantle, suggesting that the fault zone may penetrate through the crust into the upper mantle. This low-V anomaly may be caused by fluids rising from the upper mantle and then intruding upward along its broken section. An obvious low-V anomaly is observed under the 2003 Dayao earthquake source areas, implying that fluids may enter the fractured fault zone and decrease the friction of the fault, which may lead to failure of a strong asperity and triggering of these two earthquakes. The fluids may be associated with the dehydration of the subducted Indian slab in the mantle transition zone. Our tomographic result is significantly improved compared to previous studies and provides new constraints on the dynamics of the India-Asia collision. Further efforts should be made to deploy portable seismic stations to the west of Yunnan and across the fault zones in Yunnan so that the 3-D crust and upper mantle structure can be determined more accurately, and our understanding of the collision process of the Indian and Eurasian plates can be improved.

[32] **Acknowledgments.** We thank R. Engdahl for providing the hypocentral parameters he determined for the teleseismic events used in this study. We are grateful to the members of the Seismological Bureau of Yunnan Province for their help at the data-processing stage. We also thank Bernhard Steinberger, Y. Liu, and J. Liu for thoughtful discussions. This work was partially supported by grants from the National Natural Science Foundation of China (40774044) to J. Lei and a research grant (Kiban-A 17204037) from the Japanese Ministry of Education and Science to D. Zhao. The GMT software package distributed by *Wessel and Smith* [1995] was used for plotting the figures. Patrick Taylor, the Associate Editor, and two anonymous referees provided thoughtful comments and suggestions, which improved the manuscript.

## References

Abdelwahed, M., and D. Zhao (2007), Deep structure of the Japan subduction zone, *Phys. Earth Planet. Inter.*, *162*, 32–52, doi:10.1016/j.pepi.2007.03.001.

Deng, Q., P. Zhang, Y. Ran, X. Yang, W. Mi, and Q. Chu (2002), General characteristics of China active tectonics, *Sci. China, Ser. D*, *32*(12), 1021–1030.

Dziewonski, A., and F. Gilbert (1976), The effect of small aspherical perturbations on travel times and a re-examination of the corrections for ellipticity, *Geophys. J. R. Astron. Soc.*, *44*, 7–17.

Eberhart-Phillips, D. (1986), Three-dimensional velocity structure in Northern California Coast Ranges from inversion of local earthquake arrival times, *Bull. Seismol. Soc. Am.*, *76*, 1025–1052.

Engdahl, R., R. van der Hilst, and R. Buland (1998), Global teleseismic earthquake relocation with improved travel times and procedures for depth determination, *Bull. Seismol. Soc. Am.*, *88*, 722–743.

England, P., and G. Houseman (1986), Finite strain calculations of continental deformation: 2. Comparison with the India-Asia collision zone, *J. Geophys. Res.*, *91*, 3664–3676, doi:10.1029/JB091iB03p03664.

Fan, C., and Y. Cheng (1992), The crustal structure of western Yunnan, in *Geophysical Studies of Yunnan Province* (in Chinese), pp. 102–109, Yunnan Univ. Press, Kunming, China.

Fishwick, S. (2006), Gradient maps: A tool in the interpretation of tomographic images, *Phys. Earth Planet. Inter.*, *156*, 152–157, doi:10.1016/j.pepi.2006.02.003.

Harrison, T., W. Chen, P. Leloup, and F. Ryerson (1992), An early Miocene transition in deformation regime within the Red River fault zone, Yunnan, and its significance for the Indo-Asian tectonics, *J. Geophys. Res.*, *97*, 7159–7182, doi:10.1029/92JB00109.

Harrison, T., P. Leloup, F. Ryerson, P. Tapponnier, R. Lacassion, and W. Chen (1996), Diachronous initiation of transtension along the Ailao Shan–Red–River shear zone, Yunnan and Vietnam, in *The Tectonic Evolution of Asia*, edited by A. Yin and T. Harrison, pp. 208–226, Cambridge Univ. Press, New York.

Hauksson, E., and J. Haase (1997), Three-dimensional Vp and Vp/Vs velocity models of the Los Angeles basin and central Transverse Ranges, California, *J. Geophys. Res.*, *102*, 5423–5453, doi:10.1029/96JB03219.

He, H., G. He, and Y. Chen (2005), Earthquake sequences of the 2003 Dayao earthquakes (M 6.2 and 6.1), *J. Seismol. Res.*, *28*(1), 12–17.

Hickman, S., R. Sibson, and R. Bruhn (1995), Introduction to special section: Mechanical involvement of fluids in faulting, *J. Geophys. Res.*, *100*, 12,831–12,840, doi:10.1029/95JB01121.

Hu, J., Y. Hu, J. Xia, Y. Chen, H. Zhao, and H. Yang (2008), Crust-mantle velocity structure of S wave and dynamic process beneath Burma Arc and its adjacent regions, *Chin. J. Geophys.*, *51*(1), 140–148.

Hua, W., J. Liu, S. Zheng, and Z. Chen (2006), Characteristics of seismic sequences and triggering of the 2003 Dayao, Yunnan earthquakes (M 6.2 and 6.1), *Earthquake Res. China*, *22*(1), 10–22.

Huang, J., and D. Zhao (2006), High-resolution mantle tomography of China and surrounding regions, *J. Geophys. Res.*, *111*, B09305, doi:10.1029/2005JB004066.

Huang, J., D. Zhao, and S. Zheng (2002), Lithospheric structure and its relationship to seismic and volcanic activity in southwest China, *J. Geophys. Res.*, *107*(B10), 2255, doi:10.1029/2000JB000137.

Humphreys, E., and R. Clayton (1988), Adaptation of back projection tomography to seismic travel time problems, *J. Geophys. Res.*, *93*, 1073–1085, doi:10.1029/JB093iB02p01073.

Hung, S., Y. Shen, and L. Chiao (2004), Imaging seismic velocity structure beneath the Iceland hot spot: A finite frequency approach, *J. Geophys. Res.*, *109*, B08305, doi:10.1029/2003JB002889.

Iwamori, H. (1998), Transportation of $H_2O$ and melting in subduction zones, *Earth Planet. Sci. Lett.*, *160*, 65–80, doi:10.1016/S0012-821X(98)00080-6.

Kan, R., and Z. Lin (1986), A preliminary study on the crustal and upper mantle structure in Yunnan (in Chinese), *Earthquake Res. China*, *2*(4), 50–61.

Kennett, B. L. N., and E. Engdahl (1991), Traveltimes for global earthquake location and phase identification, *Geophys. J. Int.*, *105*, 429–465, doi:10.1111/j.1365-246X.1991.tb06724.x.

Lebedev, S., S. Chevrot, G. Nolet, and R. van der Hilst (2000), New seismic evidence for a deep mantle origin of the S. China basalts (the Hainan

plume?) and other observations in SE Asia, *Eos Trans. AGU*, *81*(48), Fall Meet. Suppl., Abstract T61B-13.
Lee, T., and L. Lawver (1995), Cenozoic plate reconstruction of Southeast Asia, *Tectonophysics*, *251*, 85–138, doi:10.1016/0040-1951(95)00023-2.
Lei, J., and D. Zhao (2005), P wave tomography and origin of the Changbai intraplate volcano in Northeast Asia, *Tectonophysics*, *397*, 281–295, doi:10.1016/j.tecto.2004.12.009.
Lei, J., and D. Zhao (2006a), Global P wave tomography: On the effect of various mantle and core phases, *Phys. Earth Planet. Inter.*, *154*, 44–69, doi:10.1016/j.pepi.2005.09.001.
Lei, J., and D. Zhao (2006b), A new insight into the Hawaiian plume, *Earth Planet. Sci. Lett.*, *241*, 438–453, doi:10.1016/j.epsl.2005.11.038.
Lei, J., and D. Zhao (2007a), Teleseismic evidence for a break-off subducting slab under Eastern Turkey, *Earth Planet. Sci. Lett.*, *257*, 14–28, doi:10.1016/j.epsl.2007.02.011.
Lei, J., and D. Zhao (2007b), Teleseismic P wave tomography and the upper mantle structure of the central Tienshan orogenic belt, *Phys. Earth Planet. Inter.*, *162*, 165–185, doi:10.1016/j.pepi.2007.04.010.
Lei, J., and H. Zhou (2002), 3-D P wave velocity structure of the upper mantle beneath Southwestern China and its adjacent areas, *Acta Seismol. Sin.*, *15*(2), 134–142.
Lei, J., F. Xie, C. Lan, C. Xing, and S. Ma (2008), Seismic images under the Beijing region inferred from P and PmP data, *Phys. Earth Planet. Inter.*, *168*, 134–146, doi:10.1016/j.pepi.2008.06.005.
Lei, J., D. Zhao, B. Steinberger, B. Wu, F. Shen, and Z. Li (2009), New seismic constraints on the upper mantle structure of the Hainan plume, *Phys. Earth Planet. Inter.*, *173*, 33–50, doi:10.1016/j.pepi.2008.10.013.
Leloup, P., R. Lacassin, P. Tapponnier, U. Scharer, D. Zhong, X. Liu, L. Zhang, S. Ji, and P. Trinh (1995), The Ailao Shan-Red River shear zone (Yunnan, China): Tertiary transform boundary of Indochina, *Tectonophysics*, *251*, 3–84, doi:10.1016/0040-1951(95)00070-4.
Li, C., R. van der Hilst, A. Meltzer, and E. Engdahl (2008a), Subduction of the Indian lithosphere beneath the Tibetan Plateau and Burma, *Earth Planet. Sci. Lett.*, *274*, 157–168, doi:10.1016/j.epsl.2008.07.016.
Li, Y., Q. Wu, R. Zhang, X. Tian, and R. Zeng (2008b), The crust and upper mantle structure beneath Yunnan from joint inversion of receiver functions and Rayleigh wave dispersion data, *Phys. Earth Planet. Inter.*, *170*, 134–146, doi:10.1016/j.pepi.2008.08.006.
Mishra, O. P., and D. Zhao (2003), Crack density, saturation rate and porosity at the 2001 Bhuj, India, earthquake hypocenter: A fluid-driven earthquake?, *Earth Planet. Sci. Lett.*, *212*, 393–405, doi:10.1016/S0012-821X(03)00285-1.
Montelli, R., G. Nolet, F. Dahlen, G. Masters, E. Engdahl, and S. Hung (2004), Finite-frequency tomography reveals a variety of plumes in the mantle, *Science*, *303*, 338–343, doi:10.1126/science.1092485.
Paige, C., and M. Saunders (1982), LSQR: An algorithm for sparse linear equations and sparse least squares, *Trans. Math. Software*, *8*, 43–71, doi:10.1145/355984.355989.
Peacock, S. (1990), Fluid processes in subduction zones, *Science*, *248*, 329–345, doi:10.1126/science.248.4953.329.
Qin, J., G. Huangfu, and J. Zhang (1998), Characteristics of Q values around Tengchong volcano and adjacent areas, *J. Seismol. Res.*, *21*, 358–361.
Scharer, U., P. Tapponnier, R. Lacassin, P. Leloup, D. Zhong, and S. Ji (1990), Intraplate tectonics in Asia: A precise age for Tertiary large-scale Miocene movement along the Ailao Shan-Red River shear zone, China, *Earth Planet. Sci. Lett.*, *97*, 65–77, doi:10.1016/0012-821X(90)90099-J.
Scharer, U., L. Zhang, and P. Tapponnier (1994), Duration of strike-slip movements in large shear zones: The Red River belt, China, *Earth Planet. Sci. Lett.*, *126*, 379–397, doi:10.1016/0012-821X(94)90119-8.
Shangguan, Z., C. Bai, and M. Song (2000), Mantle-derived magmatic gas releasing features at Rehai area, Tengchong county, Yunnan province, China, *Sci. China, Ser. D*, *43*(2), 132–140.
Shen, X., H. Zhou, and H. Kawakatsu (2008), Mapping the upper mantle discontinuities beneath China with teleseismic receiver functions, *Earth Planets Space*, *60*, 713–719.
Sibson, R. (1982), Fault zone models, heat flow and the depth distribution of earthquakes in the continental crust of the United States, *Bull. Seismol. Soc. Am.*, *72*, 151–163.
Sibson, R. (1992), Implications of fault-value behavior for rupture nucleation and recurrence, *Tectonophysics*, *211*, 283–293, doi:10.1016/0040-1951(92)90065-E.
Su, Y. (2004), A review and discussion on the July 21, 2003 earthquake (M 6.2) and the October 16, 2003 earthquake (M 6.1), *Recent Dev. World Seismol.*, *301*(1), 18–21.
Sun, J., C. Xu, and Z. Jiang (1989), Electricity structure of the crust and upper mantle in western Yunnan and its relation to crust activity, *Seismol. Geol.*, *11*(1), 35–49.
Tapponnier, P., et al. (1981), The Tibetan side of the India-Eurasian collision, *Nature*, *294*, 405–410, doi:10.1038/294405a0.
Tapponnier, P., R. Lacassin, P. Leloup, U. Scharer, D. Zhong, H. Wu, X. Liu, S. Ji, L. Zhang, and J. Zhong (1990), The Ailao Shan/Red-River metamorphic belt: Tertiary left-lateral shear between Indochina and South China, *Nature*, *343*, 431–437, doi:10.1038/343431a0.
Tatsumi, Y. (1989), Migration of fluid phases and genesis of basalt magmas in subduction zones, *J. Geophys. Res.*, *94*, 4697–4707, doi:10.1029/JB094iB04p04697.
Waldhauser, F., and W. Ellsworth (2000), A double-difference earthquake location algorithm: Method and application to the Northern Hayward fault, California, *Bull. Seismol. Soc. Am.*, *90*, 1353–1368, doi:10.1785/0120000006.
Wang, C., and G. Huangfu (2004), Crustal structure in Tengchong volcano-geothermal area, western Yuannan, China, *Tectonophysics*, *380*, 69–87, doi:10.1016/j.tecto.2003.12.001.
Wang, C., W. Chan, and W. Mooney (2003), Three-dimensional velocity structure of crust and upper mantle in southwestern China and its tectonic implications, *J. Geophys. Res.*, *108*(B9), 2442, doi:10.1029/2002JB001973.
Wang, E., and B. Burchfiel (1997), Interpretation of Cenozoic tectonics in the right-lateral accommodation zone between the Ailao Shan shear zone and the eastern Himalayan syntaxis, *Int. Geol. Rev.*, *39*, 191–219.
Wang, E., B. Burchfiel, L. Royden, Z. Chen, J. Chen, W. Li, and Z. Chen (1998), Late Cenozoic Xianshuihe-Xiaojiang, Red River, and Dali fault systems of southwestern Sichuan and central Yunnan, China, *Spec. Pap. Geol. Soc. Am.*, *327*, 1–108.
Wang, J., A. Yin, T. Harrison, M. Grove, Y. Zhang, and G. Xie (2001), A tectonic model for Cenozoic igneous activities in the eastern Indo-Asian collision zone, *Earth Planet. Sci. Lett.*, *188*, 123–133, doi:10.1016/S0012-821X(01)00315-6.
Wang, W., L. Chen, Q. Chen, and J. Liu (2007), Seismic velocity and attenuation structures of the 2003 Dayao earthquake source areas, *Chin. J. Geophys.*, *50*, 770–779.
Wang, Z., and D. Zhao (2006), Seismic evidence for the influence of fluids on the 2005 west off Fukuoka prefecture earthquake in southwest Japan, *Phys. Earth Planet. Inter.*, *155*, 313–324, doi:10.1016/j.pepi.2006.01.006.
Wessel, P., and W. Smith (1995), New version of the generic mapping tools released, *Eos Trans. AGU*, *76*(33), 329, doi:10.1029/95EO00198.
Wu, Q., J. Zu, and Y. Xie (1988), Basical geothermal characteristics in Yunnan Province, *Seismol. Geol.*, *10*(4), 177–183.
Xu, L., S. Rondenay, and R. van der Hilst (2007), Structure of the crust beneath the southeastern Tibetan Plateau from teleseismic receiver functions, *Phys. Earth Planet. Inter.*, *165*, 176–193, doi:10.1016/j.pepi.2007.09.002.
Xu, M., L. Wang, J. Liu, K. Zhong, H. Li, D. Hu, and Z. Xu (2005), Crust and uppermost mantle structure from receiver function analyses, *Sci. China, Ser. D*, *35*, 729–737.
Xu, Y., J. Liu, F. Liu, H. Song, T. Hao, and W. Jiang (2003), The crust and upper mantle structure of the Ailaoshan-Red River fault and adjacent areas, *Sci. China, Ser. D*, *33*, 1201–1208.
Yao, H., R. van der Hilst, and M. de Hoop (2006), Surface-wave array tomography in SE Tibet from ambient seismic noise and two-station analysis: 1. Phase velocity maps, *Geophys. J. Int.*, *166*, 732–744, doi:10.1111/j.1365-246X.2006.03028.x.
Yao, H., C. Beghein, and R. van der Hilst (2008), Surface wave array tomography in SE Tibet from ambient seismic noise and two-station analysis: 2. Crustal and upper-mantle structure, *Geophys. J. Int.*, *173*, 205–219, doi:10.1111/j.1365-246X.2007.03696.x.
Yin, A. (2000), Mode of Cenozoic east-west extension in Tibet suggesting a common origin of rifts in Asia during the Indo-Asian collision, *J. Geophys. Res.*, *105*, 21,745–21,759, doi:10.1029/2000JB900168.
Yin, A., and T. Harrison (2000), Geological evolution of the Himalayan-Tibetan orogen, *Annu. Rev. Earth Planet. Sci.*, *28*, 211–280, doi:10.1146/annurev.earth.28.1.211.
Zhao, C., R. Hua, and K. Chen (2006), Present-day magma chambers in Tengchong volcano area inferred from relative geothermal gradient, *Acta Petrol. Sin.*, *22*(6), 1517–1528.
Zhao, D. (2001), Seismic structure and origin of hotspots and mantle plumes, *Earth Planet. Sci. Lett.*, *192*, 251–265, doi:10.1016/S0012-821X(01)00465-4.
Zhao, D. (2004), Global tomographic images of mantle plumes and subducting slabs: Insight into deep Earth dynamics, *Phys. Earth Planet. Inter.*, *146*, 3–34, doi:10.1016/j.pepi.2003.07.032.
Zhao, D., and J. Lei (2004), Seismic ray path variations in a 3-D global velocity model, *Phys. Earth Planet. Inter.*, *141*, 153–166, doi:10.1016/j.pepi.2003.11.010.
Zhao, D., A. Hasegawa, and S. Horiuchi (1992), Tomographic imaging of P and S wave velocity structure beneath northeastern Japan, *J. Geophys. Res.*, *97*, 19,909–19,928, doi:10.1029/92JB00603.

Zhao, D., A. Hasegawa, and H. Kanamori (1994), Deep structure of Japan subduction zones as derived from local, regional, and teleseismic events, *J. Geophys. Res.*, *99*, 22,313–22,329, doi:10.1029/94JB01149.

Zhao, D., H. Kanamori, and H. Negishi (1996), Tomography of the source area of the 1995 Kobe earthquake: Evidence for fluids at the hypocenter?, *Science*, *274*, 1891–1894, doi:10.1126/science.274.5294.1891.

Zhao, D., O. P. Mishra, and R. Sanda (2002), Influence of fluids and magma on earthquakes: Seismological evidence, *Phys. Earth Planet. Inter.*, *132*, 249–267, doi:10.1016/S0031-9201(02)00082-1.

Zhao, D., H. Tani, and O. P. Mishra (2004), Crustal heterogeneity in the 2000 western Tottori earthquake region: Effect of fluids from slab dehydration, *Phys. Earth Planet. Inter.*, *145*, 161–177, doi:10.1016/j.pepi.2004.03.009.

Zhao, D., J. Lei, T. Inoue, A. Yamada, and S. Gao (2006), Deep structure and origin of the Baikal rift zone, *Earth Planet. Sci. Lett.*, *243*, 681–691, doi:10.1016/j.epsl.2006.01.033.

Zhong, D., et al. (1989), Huge strike-slip faults: An important style of intracontinental form after collision, *Chin. Sci. Bull.*, *7*, 526–529.

Zhou, L., J. Liu, and X. Zhang (2007), Evolution of 3-D velocity structures before the 2003 Dayao earthquakes (M 6.2 and 6.1), *Acta Seismol. Sin.*, *29*(1), 20–30.

Zhu, B., C. Mao, G. Lugmair, and J. Macdougall (1983), Isotopic and geochemical evidence for the origin of Plio-Pleistocene volcanic rocks near the Indo-Eurasian collisional margin at Tengchong, China, *Earth Planet. Sci. Lett.*, *65*, 263–275, doi:10.1016/0012-821X(83)90165-6.

J. Lei, Seismological Laboratory, Institute of Crustal Dynamics, China Earthquake Administration, Beijing 100085, China. (jshlei_cj@hotmail.com; leijs@eq-icd.cn)

Y. Su, Earthquake Administration of Yunnan Province, Kunming 650224, China.

D. Zhao, Department of Geophysics, Tohoku University, Sendai 980-8578, Japan.